BIOCHEMISTRY
including biophysical chemistry & molecular biology

Article

pubs.acs.org/biochemistry

Network of Hydrogen Bonds near the Oxygen-Evolving Mn_4CaO_5 Cluster of Photosystem II Probed with FTIR Difference Spectroscopy

Rachel J. Service,[†,§] Warwick Hillier,[‡,∥] and Richard J. Debus*[,†]

[†]Department of Biochemistry, University of California, Riverside, California 92521, United States
[‡]Research School of Biology, The Australian National University, Canberra, ACT 0200, Australia

ABSTRACT: We previously provided experimental evidence that an extensive network of hydrogen bonds exists near the oxygen-evolving Mn_4CaO_5 cluster in photosystem II and that elements of this network form part of a dominant proton-egress pathway leading from the Mn_4CaO_5 cluster to the thylakoid lumen. The evidence was based on (i) the elimination of the same ν(C═O) mode of a protonated carboxylate group in the S_2-*minus*-S_1 FTIR difference spectrum of wild-type PSII core complexes from the cyanobacterium *Synechocystis* sp. PCC 6803 by the mutations D1-E65A, D2-E312A, and D1-E329Q and (ii) the substantial decrease in the efficiency of the S_3 to S_0 transition caused by the mutations D1-D61A, D1-E65A, and D2-E312A. The eliminated ν(C═O) mode corresponds to an unidentified carboxylate group whose pK_a value decreases in response to the increased charge that develops on the Mn_4CaO_5 cluster during the S_1 to S_2 transition. In the current study, we have extended our work to include the ν(C═O) regions of other S_{n+1}-*minus*-S_n FTIR difference spectra and to additional mutations of residues inferred to participate in networks of hydrogen bonds near the Mn_4CaO_5 cluster or leading from the Mn_4CaO_5 cluster to the thylakoid lumen. Our data suggest that a different carboxylate group has its pK_a value increased during the S_2 to S_3 transition and that a third carboxylate group experiences a change in its environment during the S_0 to S_1 transition. The pK_a values that shift during the S_1 to S_2 and S_2 to S_3 transitions appear to be restored during the S_3 to S_0 transition. The D1-R334A mutation decreases or eliminates the same ν(C═O) modes from the S_2-*minus*-S_1 and S_3-*minus*-S_2 spectra as mutations D1-E65A, D2-E312A, and D1-E329Q and substantially decreases the efficiency of the S_3 to S_0 transition. We conclude that D1-R334 participates in the same dominant proton-egress pathway that was identified in our previous study. The D1-Q165E mutation leaves the ν(C═O) region of the S_2-*minus*-S_1 FTIR difference spectrum intact, but it eliminates a mode from this region of the S_3-*minus*-S_2 spectrum. We conclude that D1-Q165 participates in an extensive network of hydrogen bonds that that extends across the Mn_4CaO_5 cluster to the D1-E65/D2-E312 dyad and that includes D1-E329 and several water molecules including the W2 and W3 water ligands of the Mn_4CaO_5 cluster's dangling Mn_{A4} and Ca ions, respectively. The D2-E307Q, D2-D308N, D2-E310Q, and D2-E323Q mutations alter the ν(C═O) regions of none of the FTIR difference spectra. We conclude that these four residues are located far from the three unidentified carboxylate groups that give rise to the ν(C═O) features observed in the FTIR difference spectra.

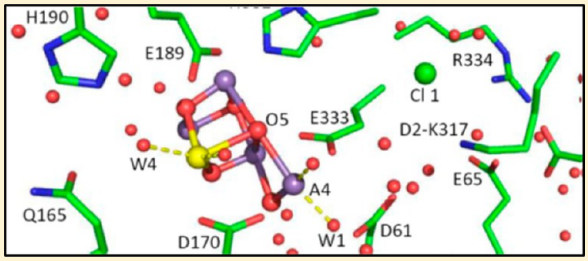

The light-driven oxidation of water in photosystem II (PSII) produces nearly all of the O_2 on earth and drives the production of nearly all of its biomass. Photosystem II is an integral membrane protein complex that is located in the thylakoid membranes of plants, algae, and cyanobacteria.[1−4] It is a homodimer *in vivo*, having a total molecular weight of approximately 700 kDa, with each monomer containing at least 20 different subunits and nearly 60 organic and inorganic cofactors including 35 Chl *a*, 11 carotenoid, two pheophytin, and two plastoquinone molecules. The O_2-evolving catalytic center in PSII consists of a Mn_4CaO_5 cluster and its immediate protein environment. In response to photochemical events within PSII, the Mn_4CaO_5 cluster accumulates four oxidizing equivalents and then catalyzes the oxidation of two molecules of water, releasing one molecule of O_2 as a byproduct.[5−9] The Mn_4CaO_5 cluster serves as the interface between single-electron photochemistry and the four-electron process of water oxidation. The photochemical events that precede water oxidation take place in a heterodimer of two 38 to 39 kDa polypeptides known as D1 and D2. These events are initiated by the transfer of excitation energy to the photochemically active Chl *a* multimer known as P_{680} following capture of light energy by the antenna complex. Excitation of P_{680} results in the formation of the charge-separated state, $P_{680}^{\bullet+}Pheo^{\bullet-}$. This light-induced separation of charge is stabilized by the rapid oxidation of $Pheo^{\bullet-}$ by Q_A, the primary plastoquinone electron acceptor, and by the rapid reduction of $P_{680}^{\bullet+}$ by Y_Z, one of two redox-active tyrosine residues in PSII. The resulting $Y_Z^{\bullet}$ radical in turn oxidizes the Mn_4CaO_5 cluster, whereas $Q_A^{\bullet-}$ reduces the secondary plastoquinone, Q_B. Subsequent charge-separations result in further oxidation of the Mn_4CaO_5 cluster and in the two-electron reduction and protonation of Q_B to form plastoquinol, which subsequently exchanges into the mem-

Received: October 25, 2013
Revised: January 22, 2014
Published: January 27, 2014

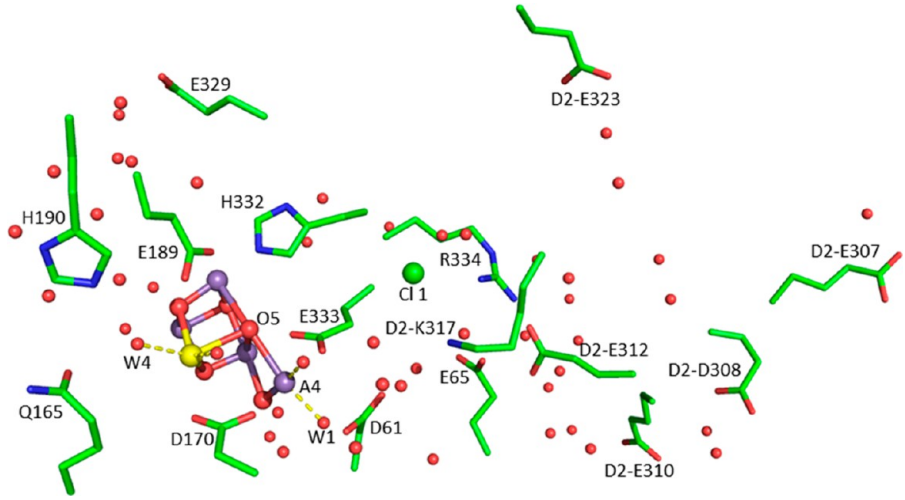

Figure 1. Positions of the residues discussed in this study in relation to the Mn_4CaO_5 cluster and selected nearby residues in the 1.9 Å structural model, including the cluster ligands D1-D170, D1-E189, D1-H332, and D1-E333.[1] Except where noted otherwise, all residues are from the D1 polypeptide. Purple spheres, manganese ions; yellow sphere, calcium; large red spheres, μ-oxo bridges; green sphere, chloride; and small red spheres, water molecules. The dangling Mn_{A4} ion, oxygen O5, and two of the cluster's water ligands (W1 and W4) are labeled.

brane-bound plastoquinone pool. During each catalytic cycle, the Mn_4CaO_5 cluster advances through five oxidation states termed S_n, where n denotes the number of oxidizing equivalents that are stored (n = 0−4). The S_1 state predominates in dark-adapted samples. The S_4 state is a transient intermediate whose formation triggers the formation and release of O_2 and the regeneration of the S_0 state.

In the recent 1.9 Å crystallographic structural model of PSII (PDB: 3ARC)[1,10] and in subsequent computational refinements of the structure of the Mn_4CaO_5 cluster and its ligation environment,[11−16] the cluster is arranged as a distorted Mn_3CaO_4 cube that is linked to a fourth dangling Mn ion (denoted Mn_{A4}) by one corner oxo bridge (denoted O5) and by an additional oxygen bridging ligand. (We have adopted the combined crystal structure and EPR-based notation for the Mn ions advanced in refs 8 and 9.) The cluster's Mn and Ca ions are ligated by six carboxylate groups and one histidine residue, all but one of which are supplied by the D1 polypeptide. In recent proposals for the mechanism of O−O bond formation, O5 derives from one of the two substrate water molecules and becomes incorporated into the product dioxygen molecule by reacting with another substrate water-derived Mn or Ca ligand.[8,9,17−22] Recent pulsed EPR studies conducted in combination with measurements of water-exchange rates have provided support for these proposals by providing strong evidence that O5 corresponds to the slowly exchanging substrate water molecule.[20,22] Structural flexibility of the Mn_4CaO_5 cluster is a key aspect of these proposals, and there is an emerging consensus that the Mn_4CaO_5 cluster readily interconverts between two nearly isoenergetic conformers during the S-state cycle, with O5 ligating the dangling Mn_{A4} ion in one conformer (giving rise to the multiline EPR signal in the S_2 state) and ligating Mn_{D1} in the other (giving rise to the g = 4.1 EPR signal in the S_2 state).[8,9,14,16,23,24] In the S_2 state, this interconversion is linked to a redox isomerization, with the Mn ion not binding O5 being in its Mn(III) oxidation state in addition to having an open coordination position along its Jahn−Teller axis. A similar structural conversion involving changes in the ligation of O5 during the S_2 to S_3 transition has also been proposed on the basis of a recent Mn-EXAFS study.[25]

Water oxidation in PSII involves a precisely choreographed sequence of proton and electron transfer steps in which the release of protons is required to prevent the redox potential of the Mn_4CaO_5 cluster from rising to levels that prevent its subsequent oxidation by $Y_Z^{\bullet}$.[26−30] This choreography is characterized by a strictly alternating removal of electrons and protons from the Mn_4CaO_5 cluster during the S-state cycle, with proton transfer preceding the oxidation of the Mn_4CaO_5 cluster during the S_2 to S_3 and S_3 to S_4 transitions.[7,19,27,28,30,31] During the S_2 to S_3 and S_3 to S_4 transitions, the trigger for proton transfer is proposed to be the formation of $Y_Z^{\bullet}$, with the positive charge on the $Y_Z^{\bullet}$/D1-His190 pair inducing the deprotonation of CP43-Arg357[26,29,32,33] or a nearby cluster of water molecules.[31] In these proposals, the subsequent oxidation of the Mn_4CaO_5 cluster involves the simultaneous transfer of a proton from the Mn_4CaO_5 cluster to the now deprotonated CP43-Arg357 or water cluster. The deprotonation of CP43-Arg357 (or the cluster of water molecules) is envisioned to take place via one or more proton-egress pathways (or channels) leading from the Mn_4CaO_5 cluster to the thylakoid lumen. The channels are expected to be composed of networks of hydrogen bonds involving protonatable amino acid side chains and water molecules. Several possible channels for water access, O_2 egress, and proton egress have been identified in the 1.9 Å[1,10] and earlier 3.5 to 2.9 Å[34−36] crystallographic structural models on the basis of visual examinations,[1,34,37−40] electrostatic calculations,[41] solvent-accessibility simulations,[42] cavity searching algorithms,[36,43,44] molecular dynamics simulations of water diffusion,[45−47] and the identification of oxidatively modified amino acid residues in the interior of PSII.[48,49] (For review, see refs 40 and 50−52.)

In an initial attempt to verify the proposed egress channels experimentally, we previously provided evidence for a network of hydrogen bonds, some elements of which may exist only transiently, that extends at least 20 Å across the lumenal face of the Mn_4CaO_5 cluster and that forms part of a dominant proton-egress pathway leading from the cluster to the lumen.[53] This network includes the residues D1-D61, D1-E65, D1-E329, and D2-E312. The evidence was based on (i) the elimination of the same ν(C═O) mode of a protonated carboxylate group in the

dx.doi.org/10.1021/bi401450y | *Biochemistry* 2014, 53, 1001−1017

S_2-*minus*-S_1 FTIR difference spectrum of wild-type PSII core complexes by the mutations D1-E65A, D2-E312A, and D1-E329Q (and by overdehydration of wild-type samples) and (ii) on the substantial decrease in the efficiencies of the S_3 to S_0 transition caused by the mutations D1-D61A, D1-E65A, and D2-E312A. The eliminated ν(C=O) mode corresponds to an unidentified carboxylate group in the same network whose pK_a value decreases in response to the increased charge that develops on the Mn_4CaO_5 cluster during the S_1 to S_2 transition. Disruption of part of this network by mutation or overdehydration prevents the transmission of the structural perturbations associated with the S_1 to S_2 transition to the unidentified carboxylate residue, thereby eliminating the pK_a change and consequently the ν(C=O) mode.

In the current study, in a further attempt to verify the proposed proton-egress channels experimentally, we have extended our previous work to include the ν(C=O) regions of the other S_{n+1}-*minus*-S_n FTIR difference spectra and to additional residues inferred to participate in networks of hydrogen bonds near the Mn_4CaO_5 cluster or leading from the Mn_4CaO_5 cluster to the thylakoid lumen (Figure 1). These include residues D1-R334, D1-Q165, D2-E307, D2-D308, D2-E310, and D2-E323. We found that (i) in addition to the carboxylic acid group whose pK_a value decreases during the S_1 to S_2 transition, there is a second carboxylic acid group whose pK_a value increases during the S_2 to S_3 transition and a third carboxylic acid group that experiences a change in its environment during the S_0 to S_1 transition, (ii) D1-R334 participates in the same dominant proton-egress pathway as D1-D61, D1-E65, and D2-E312, (iii) D1-Q165 participates in an extensive network of hydrogen bonds that that extends across the Mn_4CaO_5 cluster to the D1-E65/D2-E312 dyad and that includes several water molecules including the W2 and W3 water ligands of the dangling Mn_{A4} and Ca ions, respectively, and (iv) D2-E307, D2-D308, D2-E310, and D2-E312 are located far from the three unidentified carboxylate groups that give rise to the ν(C=O) features.

MATERIALS AND METHODS

Construction of Mutants and Propagation of Cultures. The D1-Q165E and D1-R334A mutations were constructed in the *psbA-2* gene of *Synechocystis* sp. PCC 6803[54] and transformed into a host strain of *Synechocystis* that lacks all three *psbA* genes and contains a hexahistidine-tag (His-tag) fused to the C-terminus of CP47.[55] Single colonies were selected for the ability to grow on solid media containing 5 μg/mL of kanamycin monosulfate. The D2-E307Q, D2-D308N, D2-E310Q, and D2-E323Q mutations were constructed in the *psbD-1* gene of *Synechocystis* sp. PCC 6803[56] and transformed into a host strain of *Synechocystis* that lacks both *psbD* genes[57] and contains a hexahistidine-tag (His-tag) fused to the C-terminus of CP47.[55] Single colonies were also selected for the ability to grow on solid media containing 5 μg/mL of kanamycin monosulfate. Solid media contained 5 mM glucose and 10 μM DCMU. The DCMU and antibiotic were omitted from the liquid cultures. Large-scale liquid cultures (each consisting of three 7 L cultures held in glass carboys) were propagated as described previously.[58] To verify the integrity of the mutant cultures that were harvested for the purification of PSII core complexes, an aliquot of each culture was set aside, and the sequence of the relevant portions of the *psbA-2* or *psbD-1* genes were obtained after PCR amplification of genomic DNA.[54] No traces of the wild-type codon was detected in any of the mutant cultures.

Purification of Thylakoid Membranes. Thylakoid membranes were isolated under dim green light at 4 °C with a procedure[59] modified from that of Tang and Diner.[60] Harvested cells were concentrated and suspended in a buffer containing 1.2 M betaine, 10% (v/v) glycerol, 50 mM MES-NaOH (pH 6.0), 5 mM $CaCl_2$, 5 mM $MgCl_2$, 1 mM benzamidine, 1 mM ε-amino-*n*-caproic acid, 1 mM phenymethylsulfonyl fluoride, and 0.05 mg/mL of DNase I and then broken by nine cycles of (5 s on/15 min off) in a glass-bead homogenizer (Bead-Beater, BioSpec Products, Bartlesville, OK). (The use of betaine was suggested to us by ref 61.) After separation of unbroken cells and debris by low-speed centrifugation, the resulting thylakoid membranes were concentrated by ultracentrifugation (20 min at 40 000 rpm in a Beckman Ti45 rotor) and suspended to a concentration of 1.0−1.5 mg of Chl/mL in TM buffer (1.2 M betaine, 10% (v/v) glycerol, 50 mM MES-NaOH (pH 6.0), 20 mM $CaCl_2$, 5 mM $MgCl_2$). The concentrated thylakoid membranes were used immediately for the purification of PSII core complexes.

Purification of PSII Core Complexes. Oxygen-evolving PSII core complexes were purified under dim green light at 4 °C as described previously.[59] To a suspension of freshly prepared thylakoid membranes (60−100 mg of Chl) was added the detergent *n*-dodecyl β-D-maltoside (Anatrace Inc., Maumee, OH) dropwise with gentle stirring from a stock of 10% (w/v) detergent (dissolved in TM buffer) to final concentrations of 1 mg of Chl/mL and 1% (w/v) detergent.[60] Extraction was allowed to proceed with gentle stirring for an additional 10 min in darkness. Unsolubilized material was pelleted by centrifuging at 17 500 rpm in a Beckman JA-20 rotor for 10 min.[62] The supernatant was loaded at a flow rate of 2.5 mL/min onto 40 mL of Ni-NTA superflow affinity resin (Qiagen, Inc., Valencia, CA) that had been packed in a 5 cm diameter chromatography column and equilibrated with PSII buffer (1.2 M betaine, 10% (v/v) glycerol, 50 mM MES-NaOH (pH 6.0), 20 mM $CaCl_2$, 5 mM $MgCl_2$, and 0.03% (w/v) *n*-dodecyl β-D-maltoside). After loading, the column was washed at a flow rate of 5 mL/min with four bed volumes of PSII buffer and then eluted at the same flow rate with four bed volumes of PSII buffer containing 50 mM histidine. The eluent was brought to 1 mM EDTA and concentrated by ultrafiltration (Amicon models 2000 and 8400 stirred cells fitted with YM-100 membranes followed by Amicon Ultra-4 100 K centrifugal filter devices (EMD Millipore, Billerica, MA)) to approximately 1 mg of Chl/mL. The purified PSII core complexes (in 1.2 M betaine, 10% (v/v) glycerol, 50 mM MES-NaOH (pH 6.0), 20 mM $CaCl_2$, 5 mM $MgCl_2$, 50 mM histidine, 1 mM EDTA, and 0.03% (w/v) *n*-dodecyl β-D-maltoside) were aliquotted, frozen in liquid N_2, and stored at −196 °C (vapor-phase nitrogen).

Preparation of FTIR Samples. All manipulations were conducted under dim green light at 4 °C. Samples (50 μg of Chl *a*) were exchanged into FTIR analysis buffer (40 mM sucrose, 10 mM MES-NaOH (pH 6.0), 5 mM $CaCl_2$, 5 mM NaCl, and 0.06% (w/v) *n*-dodecyl β-D-maltoside[63,64]) by passage through a centrifugal gel filtration column at 27*g*.[65] They were then concentrated to 3.3 mg of Chl/mL with Amicon Ultra-0.5 mL 100 K centrifugal filter devices (EMD Millipore, Billerica, MA). Concentrated samples (6 μL in volume) were mixed with 1:10 volume of fresh 100 mM potassium ferricyanide (dissolved in water), spread to a diameter of about 13 mm in the center of a 25 × 2 mm

dx.doi.org/10.1021/bi401450y | *Biochemistry* 2014, 53, 1001−1017

diameter BaF_2 window, then dried lightly (until tacky) under a stream of dry nitrogen gas. To maintain the sample at 99% relative humidity in the FTIR sample compartment, four 1 μL drops of a solution of 20% (v/v) glycerol in water were spotted around the periphery of the window, not touching the sample.[66] A second BaF_2 window was placed over the first, with a 23 × 1 mm nitrile O-ring acting as a spacer. The sample assembly was sealed into an aluminum cell, loaded into a water-jacketed aluminum holder in the FTIR sample compartment, and allowed to equilibrate in darkness for 2 h. The sample was kept at a constant temperature of 0 °C by circulating a cold solution of 50% (v/v) ethylene glycol in water through the sample cell holder. Sample concentrations were adjusted so that the absolute absorbance of the amide I band at 1657 cm^{-1} was 0.8−1.2. For measurements in D_2O, the FTIR analysis buffer and the potassium ferricyanide and glycerol solutions were prepared with D_2O (99.9% enrichment, Cambridge Isotope Laboratories, Andover, MA). The pD of the FTIR analysis buffer prepared in D_2O was adjusted with freshly opened NaOD (99.5% enrichment, Cambridge Isotope Laboratories, Andover, MA). The pD value was obtained by adding 0.40 to the pH meter reading.[67,68]

FTIR Spectra. Midfrequency FTIR spectra were recorded with a Bruker Vertex 70 spectrometer (Bruker Optics, Billerica, MA) that was equipped with a KBr beam splitter and a preamplified, midrange D317 photovoltaic MCT detector (Kolmar Technologies, Inc., Newburyport, MA). Long-pass 2.4 μm cutoff filters (Andover Corp., Salem, NH) were mounted on both sides of the sample compartment to prevent the interferometer's coaxial helium−neon laser from illuminating the sample and to protect the MCT detector from scattered actinic illumination. Double-sided forward−backward interferograms were recorded with a scanner velocity of 120 kHz. For the calculation of Fourier transforms, a Blackman−Harris three-term apodization function and a zero-fill factor of 2 were employed. The spectral resolution for all spectra was 4 cm^{-1}. Actinic illumination consisted of flashes (~ 20 mJ/flash, ~ 7 ns fwhm) provided by a frequency-doubled Q-switched Nd:YAG laser (BRIO (Quantel USA, Bozeman, MT)). Flash excitation was controlled from the Vertex 70 OPUS interface. The Nd:YAG laser was programmed to deliver a single Q-switched flash during a 20 Hz flashlamp repetition series to ensure the uniformity of the laser light intensity. For each sample, after dark adaptation, six successive flashes were applied with an interval of 13 s between each (no preflashes were applied). Two single-beam spectra were recorded before the first flash and one single-beam spectrum was recorded starting 0.33 s after the first and subsequent flashes (each single-beam spectrum consisted of 100 scans). The 0.33 s delay was incorporated to allow for the oxidation of $Q_A^{\bullet-}$ by the ferricyanide. To obtain difference spectra corresponding to successive S-state transitions, the single-beam spectrum that was recorded after the *n*th flash was divided by the single-beam spectrum that was recorded immediately before the *n*th flash, and the ratio was converted to units of absorption. To estimate the background noise level, the second preflash single-beam spectrum was divided by the first, and the ratio was converted to units of absorption. The sample was dark-adapted for 30 min, and then the cycle was repeated. The cycle was repeated 16 times for each sample, and the difference spectra recorded with several samples were averaged.

Normalization of spectra to the extent of flash-induced charge separation was accomplished by normalizing the mutant and wild-type spectra to the peak-to-peak amplitudes of the negative ferricyanide peak at 2115 cm^{-1} and the positive ferrocyanide peak at 2038 cm^{-1} that were produced by the oxidation of $Q_A^{\bullet-}$ by ferricyanide.

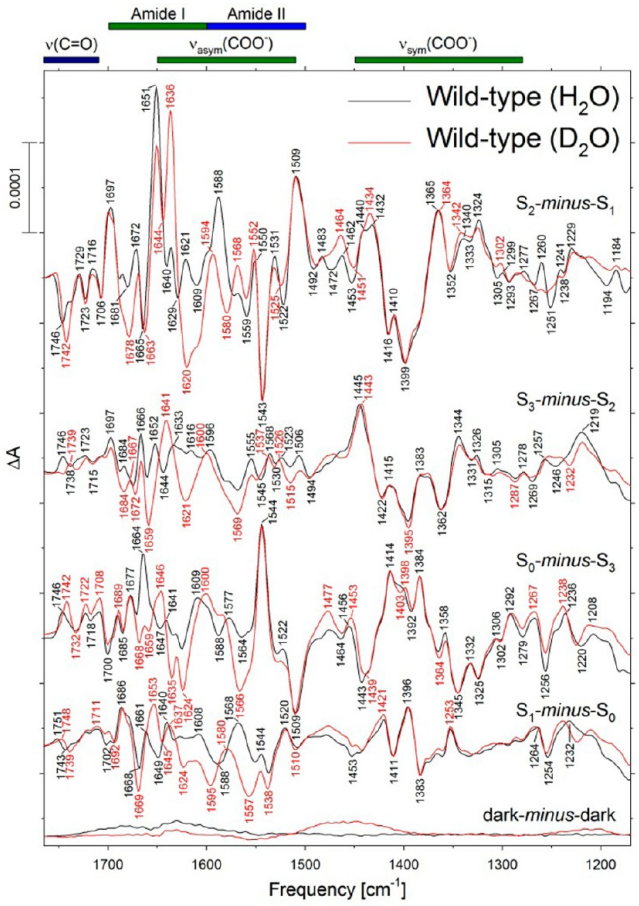

Figure 2. Comparison of the midfrequency FTIR difference spectra of wild-type PSII core complexes exchanged into FTIR buffer containing H_2O (black) or D_2O (red) in response four successive flash illuminations applied at 0 °C. The spectra (plotted from 1770 to 1170 cm^{-1}) were normalized to maximize the overlap between 1450 and 1350 cm^{-1}, and they correspond predominantly to the S_2-*minus*-S_1, S_3-*minus*-S_2, S_0-*minus*-S_3, and S_1-*minus*-S_0 FTIR difference spectra. The data represent the averages of 12 H_2O and 14 D_2O samples (14 700 and 19 380 scans for each trace, respectively). Dark-*minus*-dark control traces are included to show the noise level (lower traces).

Other Procedures. Chlorophyll concentrations and initial light-saturated rates of O_2 evolution were measured as described previously.[69]

RESULTS

ν(C═O) Region of Wild-Type PSII in H_2O and D_2O. The FTIR difference spectra induced by four successive flashes given to wild-type PSII core complexes from *Synechocystis* sp. PCC 6803 are shown in Figure 2 (black traces). The spectra that are induced by the first, second, third, and fourth flashes should correspond predominantly to S_2-*minus*-S_1, S_3-*minus*-S_2, S_0-*minus*-S_3, and S_1-*minus*-S_0 FTIR difference spectra, respectively.[70−72] The 1790−1710 cm^{-1} regions of these spectra are shown expanded in Figure 3. In this region, the S_2-*minus*-S_1 spectrum exhibits a negative band at 1746 cm^{-1} having $\Delta A = -5.4 \times 10^{-5}$, the S_3-*minus*-S_2 spectrum exhibits a positive band at 1746 cm^{-1} having $\Delta A = 1.8 \times 10^{-5}$, the S_0-*minus*-S_3

dx.doi.org/10.1021/bi401450y | *Biochemistry* 2014, 53, 1001−1017

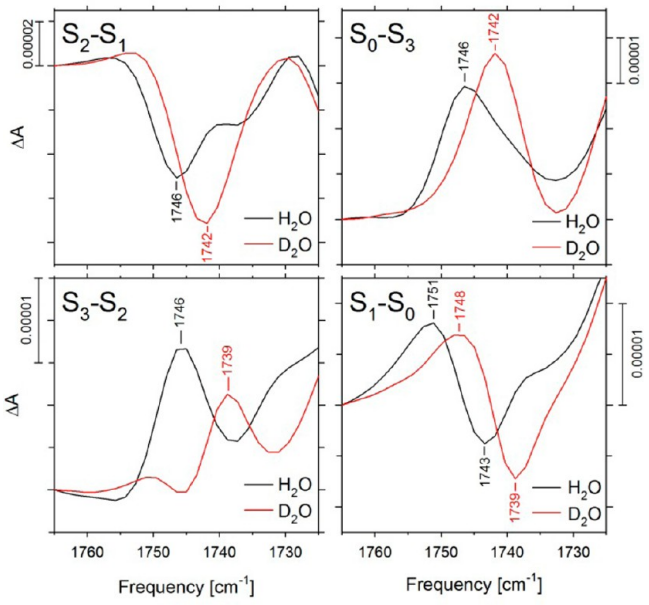

Figure 3. Comparison of the ν(C=O) regions of the S_{n+1}-*minus*-S_n FTIR difference spectra of wild-type PSII core complexes exchanged into FTIR buffer containing H_2O (black) or D_2O (red). The data are reproduced from Figure 2 but were shifted vertically to coincide at 1765 cm^{-1}. Note the different vertical scales.

spectrum exhibits a positive band at 1746 cm^{-1} having ΔA = 2.9 × 10^{-5}, and the S_1-*minus*-S_0 spectrum exhibits a derivative-shaped feature at 1751(+)/1743(−) cm^{-1} having a peak-to-peak ΔA of 1.2 × 10^{-5}. The 1790−1710 cm^{-1} region contains the C=O carbonyl stretching (ν(C=O)) modes of protonated carboxylate residues[73−75] and the keto and ester C=O vibrations of chlorophyll, pheophytin, heme, and lipids.[76] In carboxylic acids, the C=O stretching and C−O−H bending modes of the COOH group are weakly coupled. This coupling is removed by deuteration, causing the ν(C=O) mode to downshift by 4−20 cm^{-1}.[73,77−80] Accordingly, to test whether the bands in this region of the S_3-*minus*-S_2, S_0-*minus*-S_3, and S_1-*minus*-S_0 spectra correspond to the ν(C=O) modes of protonated carboxylate residues, the spectra were also obtained after samples were exchanged into buffer containing D_2O (Figures 2 and 3, red traces). In D_2O, the 1746 cm^{-1} mode in the S_2-*minus*-S_1 and S_0-*minus*-S_3 spectra appeared at 1742 cm^{-1}, the 1746 cm^{-1} mode in the S_3-*minus*-S_2 spectrum appeared at 1739 cm^{-1}, and the derivative-shaped feature in the S_1-*minus*-S_0 spectrum appeared at 1748(+)/1739(−) cm^{-1}. These represent downshifts of 3−7 cm^{-1}. Therefore, we attribute these features to the ν(C=O) modes of protonated carboxylate residues whose environments change during the individual S-state transitions (see Discussion).

Exchange into D_2O induced additional alterations to the wild-type FTIR difference spectra. In the S_2-*minus*-S_1 FTIR difference spectrum, the D_2O-induced alterations in the overlapping amide/asymmetric carboxylate stretching ($\nu_{asym}(COO^-)$) regions (between 1700 and 1500 cm^{-1}) resembled those reported previously in PSII membranes from spinach[81] and PSII core complexes from *Thermosynechococcus elongatus*[82] and *Synechocystis* sp. PCC 6803.[53] These alterations include the appearance of a positive band at 1636 cm^{-1}, the apparent upshift of a negative band from 1559 to 1580 cm^{-1}, and the apparent upshift of the large positive feature from 1588 to 1594 cm^{-1}. The first of these has been attributed to D_2O-induced shifts of amide I bands in stretches of polypeptide having random-coil conformations.[81] The second has been attributed to a D_2O-induced shift of the $\nu_{asym}(COO^-)$ mode of a carboxylate residue that accepts a strong hydrogen bond from a Mn-bound water molecule.[81] The third is consistent with the D_2O-induced upshift of the $\nu_{asym}(COO^-)$ mode of another hydrogen-bonded carboxylate residue.[81] We attribute the D_2O-induced alterations to this region of the other S_{n+1}-*minus*-S_n FTIR difference spectra primarily to D_2O-induced shifts of amide I bands in stretches of polypeptide having irregular elements of secondary structure.[75,83,84] These alterations differ somewhat from those reported previously in PSII core complexes from *T. elongatus*,[82] particularly the large 1659(−)/1641(+)/1621(−) cm^{-1} feature in the S_3-*minus*-S_2 D_2O spectrum and the negative feature at 1566 cm^{-1} in the S_0-*minus*-S_3 D_2O spectrum. We attribute these differences to small differences in elements of secondary structure between *T. elongatus* and *Synechocystis* sp. PCC 6803 arising from the slight differences in the amino acid sequences of these two organisms.

D1-R334A Mutant. Cells of the D1-R334A mutant were photoautotrophic and evolved O_2 at 190−230 μmol O_2 (mg of Chl)$^{-1}$ h^{-1} under light-saturating conditions compared to 570−580 μmol O_2 (μg of Chl)$^{-1}$ h^{-1} for wild-type cells. The O_2-evolving activities of the D1-R334A PSII core particles were approximately 2.2 mmol O_2 (mg of Chl)$^{-1}$ h^{-1} compared to 5.3−5.7 mmol O_2 (mg of Chl)$^{-1}$ h^{-1} for wild type. The O_2-evolving activity of the D1-R334A PSII core complexes (approximately 40% compared to wild type) correlated approximately with the O_2-evolving activity of D1-R334A cells (approximately 37% compared to wild type). The midfrequency FTIR difference spectra of wild-type and D1-R334A PSII core complexes that were induced by four successive flashes are compared in Figure 4 (black and red spectra, respectively). When the amplitudes of the spectra were normalized to the extent of flash-induced charge separation, the amplitudes of the D1-R334A spectra were approximately 60% of the amplitude of the wild-type spectrum. Accordingly, approximately 60% of the D1-R334A PSII core complexes were estimated to contain photo-oxidizable Mn_4CaO_5 clusters. The lower steady-state rates of O_2 evolution exhibited by D1 R334A PSII core complexes compared to their estimated content of Mn_4CaO_5 clusters implies that at least one of the S-state transitions proceeds less efficiently in the presence of the D1-R334A mutation.

The S_2-*minus*-S_1 FTIR difference spectrum of D1-R334A PSII core complexes (upper red trace in Figure 4) showed substantial differences from the wild-type spectrum throughout the midfrequency spectrum. In the amide I region, the mutation increased the amplitude of the 1698(+), 1665(−), and 1651(+) bands and upshifted (to 1675(+) cm^{-1}) and substantially increased the amplitude of the positive band at 1672(+) cm^{-1}. In the overlapping amide II/$\nu_{asym}(COO^-)$ region, the amplitudes of the bands at 1588(+), 1559(−), and 1543(−) were diminished substantially, the negative band at 1522(−) cm^{-1} was eliminated, and the positive band at 1509 cm^{-1} was upshifted to 1512 cm^{-1} and decreased in intensity. The 1543(−), 1531(+), and 1522(−) cm^{-1} bands can be identified as amide II modes because all three bands downshift appreciably after global incorporation of ^{13}C[63,85−87] or ^{15}N.[63,86−89] Similarly, the 1587 cm^{-1} band has been assigned to a $\nu_{asym}(COO^-)$ mode because it downshifts by 30−35 cm^{-1} after global incorporation of ^{13}C[63,85−87] but is largely insensitive to the global incorporation of ^{15}N.[63,86−89] The 1509 cm^{-1} band

dx.doi.org/10.1021/bi401450y | *Biochemistry* 2014, 53, 1001−1017

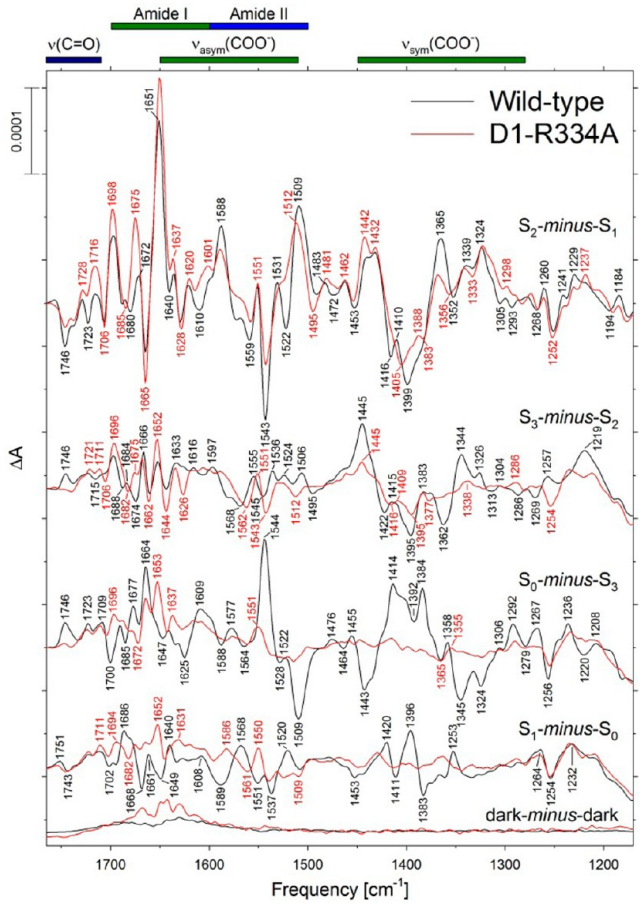

Figure 4. Comparison of the midfrequency FTIR difference spectra of wild-type (black) and D1-R334A (red) PSII core complexes in response four successive flash illuminations applied at 0 °C. The data represent the averages of 12 wild-type and nine D1-R334A samples (14 700 and 13 400 scans for each trace, respectively). The spectra were normalized to maximize the overlap between 1450 and 1350 cm^{-1} by multiplying the mutant spectra vertically by a factor of ∼1.7 after normalization to the peak-to peak amplitudes of the negative ferricyanide peak at 2115 cm^{-1} and the positive ferrocyanide peak at 2038 cm^{-1}. Dark-*minus*-dark control traces are included to show the noise level (lower traces).

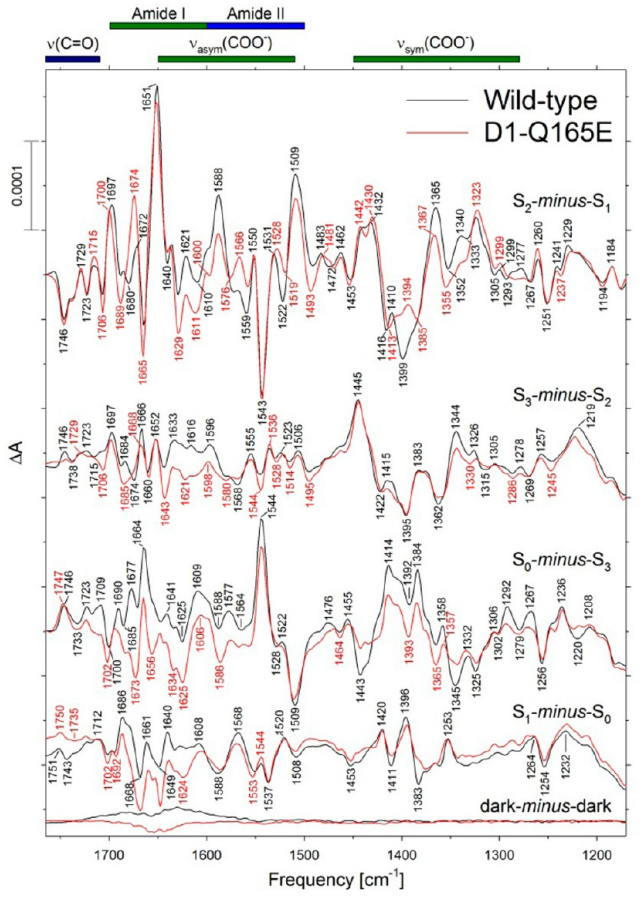

Figure 5. Comparison of the midfrequency FTIR difference spectra of wild-type (black) and D1-Q165E (red) PSII core complexes in response four successive flash illuminations applied at 0 °C. The data represent the averages of 12 wild-type and 13 D1-Q165E samples (14 700 and 17 200 scans for each trace, respectively). The spectra were normalized to maximize the overlap between 1450 and 1350 cm^{-1} by multiplying the mutant spectra vertically by a factor of ∼1.8 after normalization to the peak-to peak amplitudes of the negative ferricyanide peak at 2115 cm^{-1} and the positive ferrocyanide peak at 2038 cm^{-1}. Dark-*minus*-dark control traces are included to show the noise level (lower traces).

appears to consist of overlapping amide II and $\nu_{asym}(COO^-)$ modes.[63,86−89] In the symmetric carboxylate stretching ($\nu_{sym}(COO^-)$) region, the positive feature at 1442 cm^{-1} was intensified, the negative features at 1416 and 1399 cm^{-1} were replaced by a single negative feature at 1405 cm^{-1}, a 1388(+)/1383(−) feature appeared, and the amplitude of the large positive feature at 1365 cm^{-1} was diminished substantially. The numerous mutation-induced changes in the amide I and amide II regions show that the mutation substantially alters the response of the protein backbone to the positive charge that develops on the Mn_4CaO_5 cluster during the S_1 to S_2 transition. The many mutation-induced changes in the $\nu_{sym}(COO^-)$ shows that the mutation also perturbs multiple carboxylate residues. Of particular importance to this study, the amplitude of the negative band at 1746 cm^{-1} was decreased in amplitude by the mutation.

The FTIR difference spectrum that was produced by the second flash applied to D1-R334A PSII core complexes was much lower in amplitude than the corresponding spectrum of wild type and appeared to contain some of the features present in the S_2-*minus*-S_1 FTIR difference spectrum of this mutant (compare the upper two red traces in Figure 4). These include bands at 1675(+), 1626(−), 1551(+), 1543(−), 1338(+), and 1254(−) cm^{-1}. The presence of these bands suggests that a significant fraction of D1-R334A PSII reaction centers did not undergo the S_2 to S_3 transition following the second flash. Note that the positive band at 1746 cm^{-1} was eliminated by the mutation (see the next paragraph).

The FTIR difference spectra that were produced by the third and fourth flashes applied to D1-R334A PSII core complexes were practically devoid of features (lower two red traces in Figure 4). One possible explanation for these featureless spectra is that a large fraction of D1-R334A PSII core complexes fail to advance beyond the S_3 state. However, another possibility is that the efficiencies of the S-state transitions are substantially decreased by the mutation (i.e., that the miss parameter is increased), so that significant fractions of PSII centers fail to advance after each flash. Typically, spectral features that appear in the FTIR difference spectra during the S_1 to S_2 and S_2 to S_3 transitions are reversed during the S_3 to S_0 and S_0 to S_1

dx.doi.org/10.1021/bi401450y | *Biochemistry* 2014, 53, 1001−1017

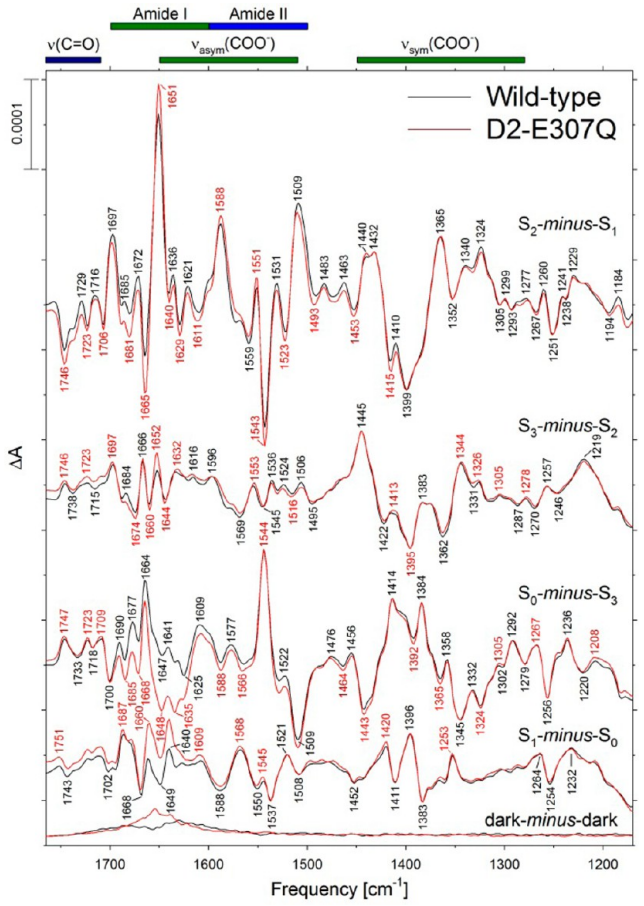

Figure 6. Comparison of the midfrequency FTIR difference spectra of wild-type (black) and D2-E307Q (red) PSII core complexes in response four successive flash illuminations applied at 0 °C. The data represent the averages of 12 wild-type and 12 D2-E307Q samples (14 700 scans for each trace). The spectra were normalized to maximize the overlap between 1450 and 1350 cm^{-1} by multiplying the mutant spectra vertically by a factor of ∼1.4 after normalization to the peak-to peak amplitudes of the negative ferricyanide peak at 2115 cm^{-1} and the positive ferrocyanide peak at 2038 cm^{-1}. Dark-*minus*-dark control traces are included to show the noise level (lower traces).

transitions.[70,71] If large fractions of PSII reaction centers fail to advance between S states in response to saturating flashes, then PSII reaction centers that undergo the S_3 to S_0 or S_0 to S_1 transitions after the third or fourth flashes may have their spectral features canceled by PSII reaction centers undergoing the S_1 to S_2 or S_2 to S_3 transitions. The apparent presence of S_2-*minus*-S_1 features in the second-flash D1-R334A spectrum and the lack of clear, distinct peaks in the third- and fourth-flash spectra are consistent with an overall increase in the miss parameter. In support of this interpretation, D1-R334A PSII core complexes evolve O_2 at substantial rates under continuous illumination (67% compared to wild type when the rate of O_2 evolution is normalized to the fraction PSII centers estimated to contain photo-oxidizable Mn_4CaO_4 clusters). Consequently, the elimination of the positive band at 1746 cm^{-1} in the S_3-*minus*-S_2 spectrum of the D1-R334A mutant may have been caused by an increased miss parameter in the mutant.

D1-Q165E Mutant. Cells of the D1-Q165E mutant were photoautotrophic and evolved O_2 at approximately 190 μmol O_2 (mg of Chl)$^{-1}$ h^{-1} under light-saturating conditions compared to 570−580 μmol O_2 (μg of Chl)$^{-1}$ h^{-1} for wild-type cells. The O_2-evolving activities of the D1-Q165E PSII core particles were approximately 1.9 mmol O_2 (mg of Chl)$^{-1}$ h^{-1} compared to 5.3−5.7 mmol O_2 (mg of Chl)$^{-1}$ h^{-1} for wild type. The O_2-evolving activity of the D1-Q165E PSII core complexes (approximately 35% compared to wild type) correlated approximately with the O_2-evolving activity of D1-Q165E cells (approximately 33% compared to wild type). The midfrequency FTIR difference spectra of wild-type and D1-Q165E PSII core complexes that were induced by four successive flashes are compared in Figure 5 (black and red spectra, respectively). When the amplitudes of the spectra were normalized to the extent of flash-induced charge separation, the amplitudes of the D1-Q165E spectra were approximately 55% of the amplitude of the wild-type spectrum. Accordingly, approximately 55% of the D1-Q165E PSII core complexes were estimated to contain photo-oxidizable Mn_4CaO_5 clusters. The lower steady-state rates of O_2 evolution exhibited by D1-Q165E PSII core complexes compared to their estimated content of Mn_4CaO_5 clusters implies that at least one of the S-state transitions proceeds less efficiently in the presence of the D1-Q165E mutation.

The S_2-*minus*-S_1 FTIR difference spectrum of D1-Q165E PSII core complexes (upper red trace in Figure 5) showed substantial differences from the wild-type spectrum throughout the midfrequency spectrum. In the amide I region, the mutation increased the amplitude of the 1706(−), 1689(−), and 1665(−) cm^{-1} bands, shifted the 1697(+) cm^{-1} peak to 1700 cm^{-1}, eliminated the small negative feature at 1680 cm^{-1}, and shifted the 1672(+) band to 1674(+) cm^{-1}, substantially increasing the amplitude of the latter. In the overlapping amide II/$\nu_{asym}(COO^-)$ region, the amplitudes of the positive bands at 1588 and 1509 cm^{-1} were diminished, the amplitudes of the negative features at 1629 and 1611 cm^{-1} were increased, a positive feature at 1566 cm^{-1} appeared, and the 1531(+)/1522(−) cm^{-1} feature was shifted to 1528(+)/1519(−) cm^{-1}. In the $\nu_{sym}(COO^-)$ region, the negative feature at 1416 cm^{-1} was shifted to 1413 cm^{-1}, the large negative feature at 1399 cm^{-1} was replaced with a positive feature at 1394 cm^{-1} (thereby obscuring the 1410(+) cm^{-1} feature and creating a negative feature at 1385 cm^{-1}), the large positive feature at 1365 cm^{-1} was upshifted to 1367 cm^{-1} and its amplitude was sharply decreased, the positive feature at 1340 cm^{-1} was largely eliminated, and the small positive feature at 1277 cm^{-1} was eliminated. The numerous mutation-induced changes in the amide I and amide II regions show that the mutation substantially alters the response of the protein backbone to the positive charge that develops on the Mn_4CaO_5 cluster during the S_1 to S_2 transition. The mutation-induced changes in the $\nu_{sym}(COO^-)$ region shows that the mutation also perturbs multiple carboxylate residues. Of particular importance to this study, the amplitude of the negative band at 1746 cm^{-1} was unchanged by the mutation.

The S_3-*minus*-S_2 FTIR difference spectrum of D1-Q165E PSII core complexes showed many fewer changes compared to wild type than the mutant's S_2-*minus*-S_1 spectrum. In the amide I region, a negative feature appeared at 1706 cm^{-1}, the positive feature at 1684 cm^{-1} was replaced by a negative feature at 1685 cm^{-1}, and the positive feature at 1666 cm^{-1} upshifted to 1668 cm^{-1} and decreased slightly in amplitude. In the overlapping amide II/$\nu_{asym}(COO^-)$ region, the negative feature at 1644 cm^{-1} was downshifted to 1643 cm^{-1} and its amplitude was increased, the positive feature at 1596 cm^{-1} was upshifted to 1598 cm^{-1}, and the amplitudes of the negative features at 1544

dx.doi.org/10.1021/bi401450y | *Biochemistry* 2014, 53, 1001−1017

and 1495 cm^{-1} were increased. In the $\nu_{sym}(COO^-)$ region, the positive features at 1415 and 1344 cm^{-1} were decreased in amplitude. Of particular importance to this study, the amplitude of the positive band at 1746 cm^{-1} was nearly eliminated by the D1-Q165E mutation.

Most of the features in the S_0-*minus*-S_3 FTIR difference spectrum of D1-Q165E PSII core complexes were diminished in amplitude compared to those in the corresponding wild-type spectrum. However, there were relatively few other changes. These changes included the elimination of the positive feature at 1709 cm^{-1}, the upshift of the negative peak at 1700 to 1702 cm^{-1}, the replacement of the positive feature at 1677 cm^{-1} with a negative feature at 1673 cm^{-1}, the appearance of a negative feature at 1656 cm^{-1}, and the near elimination of the small 1528(−)/1522(+) cm^{-1} feature (mirroring the changes in the S_2-*minus*-S_1 spectrum). The positive band at 1746 cm^{-1} was upshifted slightly to 1747 cm^{-1}, but its amplitude was unaltered.

Most of the features in the S_1-*minus*-S_0 FTIR difference spectrum of D1-Q165E PSII core complexes were also diminished in amplitude compared to those in the corresponding wild-type spectrum. As with the mutant's S_0-*minus*-S_3 spectrum, there were relatively few other changes. These include increased intensity of the negative features at 1668 and 1649 cm^{-1}, the appearance of a negative feature at 1624 cm^{-1}, a more pronounced 1553(−)/1544(+) cm^{-1} feature, and the loss of a small negative feature at 1383 cm^{-1}. Of particular importance to this study, the 1751(+)/1743(−) cm^{-1} derivative-shaped feature changed slightly in appearance, with its positive lobe at 1750 cm^{-1} and its negative lobe becoming broader, having a minimum at 1735 cm^{-1}.

The diminished amplitudes of the mutant S_0-*minus*-S_3 and S_1-*minus*-S_0 spectra compared to wild type suggests that the efficiency of the S_3 to S_0 and S_0 to S_1 transitions are lowered by the D1-Q165E mutation, perhaps explaining the lower O_2-evolving activity of this mutant compared to wild type.

D2-E307Q Mutant. Cells of the D2-E307Q mutant were photoautotrophic and evolved O_2 at 410−440 μmol O_2 (mg of Chl)$^{-1}$ h^{-1} under light-saturating conditions compared to 570−580 μmol O_2 (μg of Chl)$^{-1}$ h^{-1} for wild-type cells. The O_2-evolving activities of the D2-E307Q PSII core particles were approximately 4.4 mmol O_2 (mg of Chl)$^{-1}$ h^{-1} compared to 5.3−5.7 mmol O_2 (mg of Chl)$^{-1}$ h^{-1} for wild type. The O_2-evolving activity of the D2-E307Q PSII core complexes (approximately 80% compared to wild type) correlated with the O_2-evolving activity of D1-E307Q cells (75−85% compared to wild type). The midfrequency FTIR difference spectra of wild-type and D2-E307Q PSII core complexes that were induced by four successive flashes are compared in Figure 6 (black and red spectra, respectively). When the amplitudes of the spectra were normalized to the extent of flash-induced charge separation, the amplitudes of the D2-E307Q spectra were approximately 70% of the amplitude of the wild-type spectrum. Accordingly, approximately 70% of the D2-E307Q PSII core complexes were estimated to contain photo-oxidizable Mn_4CaO_5 clusters. This estimate correlates approximately with the steady-state rates of O_2 evolution observed in the mutant PSII core complexes, suggesting that those Mn_4CaO_5 clusters that assemble in the mutant are all active. After normalization, the S_{n+1}-*minus*-S_n FTIR Difference spectra of the D2-E307Q PSII core complexes closely resembled the corresponding spectra of wild type. Differences include a larger amplitude derivative feature at 1665(−)/1651(+) cm^{-1} and a slightly more intense negative peak at 1543 cm^{-1} in the S_2-*minus*-S_1 spectrum, more pronounced negative features at 1648 and 1635 cm^{-1} in the S_0-*minus*-S_3 spectrum, and more pronounced positive features at 1660 and 1640 cm^{-1} in the S_1-*minus*-S_0 spectrum. Of particular importance to this study, the features at 1746 cm^{-1} in the S_2-*minus*-S_1, S_3-*minus*-S_2, and S_0-*minus*-S_3 spectra and the derivative feature at 1751(+)/1743(−) cm^{-1} in the S_1-*minus*-S_0 spectrum were unaffected by the D2-E307Q mutation.

D2-D308N Mutant. Cells of the D2-D308N mutant were photoautotrophic and evolved O_2 at 310−360 μmol O_2 (mg of Chl)$^{-1}$ h^{-1} under light-saturating conditions compared to 570−580 μmol O_2 (μg of Chl)$^{-1}$ h^{-1} for wild-type cells. The O_2-evolving activities of the D2-D308N PSII core particles were approximately 3.3 mmol O_2 (mg of Chl)$^{-1}$ h^{-1} compared to 5.3−5.7 mmol O_2 (mg of Chl)$^{-1}$ h^{-1} for wild type. The O_2-evolving activity of the D2-E307Q PSII core complexes (approximately 60% compared to wild type) correlated with the O_2-evolving activity of D1-D308N cells (55−65% compared to wild type). The midfrequency FTIR difference spectra of wild-type and D2-D308N PSII core complexes that were induced by four successive flashes are compared in Figure 7 (black and red spectra, respectively). When the amplitudes of the spectra were normalized to the extent of flash-induced charge separation, the amplitudes of the D2-D308N spectra were approximately 63% of the amplitude of the wild-type spectrum. Accordingly, approximately 63% of the D2-D308N PSII core complexes were estimated to contain photo-oxidizable Mn_4CaO_5 clusters. This estimate correlates with the steady-state rates of O_2 evolution observed in the mutant PSII core complexes, suggesting that those Mn_4CaO_5 clusters that assemble in the mutant are all active. After normalization, the S_{n+1}-*minus*-S_n FTIR difference spectra of the D2-D308N PSII core complexes closely resembled the corresponding spectra of wild type. Differences include a smaller amplitude derivative feature at 1665(−)/1651(+) cm^{-1} and a slightly less intense negative peak at 1543 cm^{-1} in the S_2-*minus*-S_1 spectrum, more pronounced negative features at 1647 and 1635 cm^{-1} in the S_0-*minus*-S_3 spectrum, and the absence of a negative feature at 1649 cm^{-1} in the S_1-*minus*-S_0 spectrum. Of particular importance to this study, the features at 1746 cm^{-1} in the S_2-*minus*-S_1, S_3-*minus*-S_2, and S_0-*minus*-S_3 spectra and the derivative feature at 1751(+)/1743(−) cm^{-1} in the S_1-*minus*-S_0 spectrum were unaffected by the D2-D308N mutation with the exception of a 1 cm^{-1} downshift of the positive feature at 1746 cm^{-1} in the S_3-*minus*-S_2 spectrum.

D2-E310Q Mutant. Cells of the D2-E310Q mutant were photoautotrophic and evolved O_2 at 410−490 μmol O_2 (mg of Chl)$^{-1}$ h^{-1} under light-saturating conditions compared to 570−580 μmol O_2 (μg of Chl)$^{-1}$ h^{-1} for wild-type cells. The O_2-evolving activities of the D2-E310Q PSII core particles were approximately 4.5 mmol O_2 (mg of Chl)$^{-1}$ h^{-1} compared to 5.3−5.7 mmol O_2 (mg of Chl)$^{-1}$ h^{-1} for wild type. The O_2-evolving activity of the D2-E310Q PSII core complexes (approximately 80% compared to wild type) correlated with the O_2-evolving activity of D2-E310Q cells (70−85% compared to wild type). The midfrequency FTIR difference spectra of wild-type and D2-E310Q PSII core complexes that were induced by four successive flashes are compared in Figure 8 (black and red spectra, respectively). When the amplitudes of the spectra were normalized to the extent of flash-induced charge separation, the amplitudes of the D2-E310Q spectra were approximately 70% of the amplitude of the wild-type

dx.doi.org/10.1021/bi401450y | *Biochemistry* 2014, 53, 1001−1017

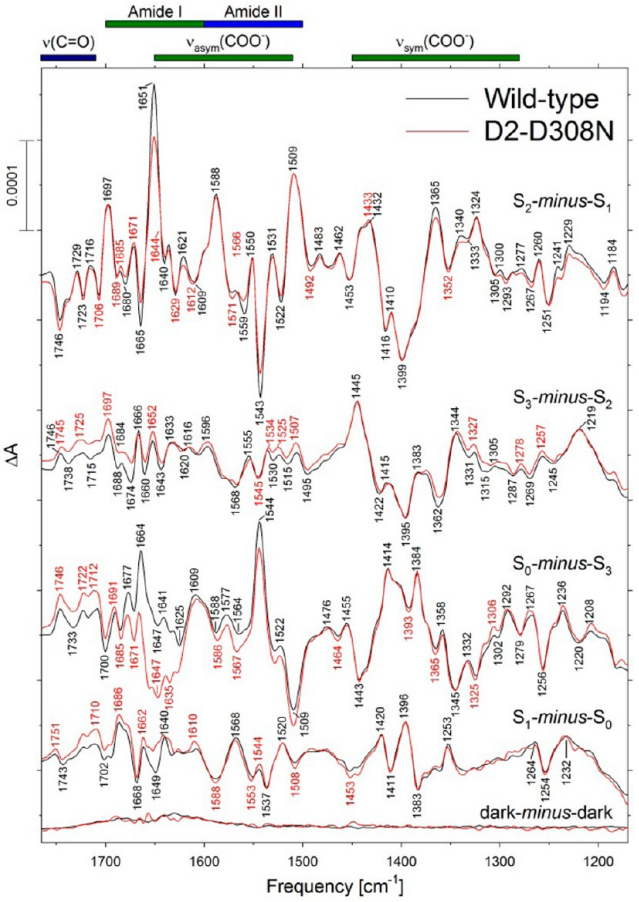

Figure 7. Comparison of the midfrequency FTIR difference spectra of wild-type (black) and D2-D308N (red) PSII core complexes in response four successive flash illuminations applied at 0 °C. The data represent the averages of 12 wild-type and five D2-D308N samples (14 700 and 6800 scans for each trace, respectively). The spectra were normalized to maximize the overlap between 1450 and 1350 cm^{-1} by multiplying the mutant spectra vertically by a factor of ∼1.6 after normalization to the peak-to peak amplitudes of the negative ferricyanide peak at 2115 cm^{-1} and the positive ferrocyanide peak at 2038 cm^{-1}. Dark-*minus*-dark control traces are included to show the noise level (lower traces).

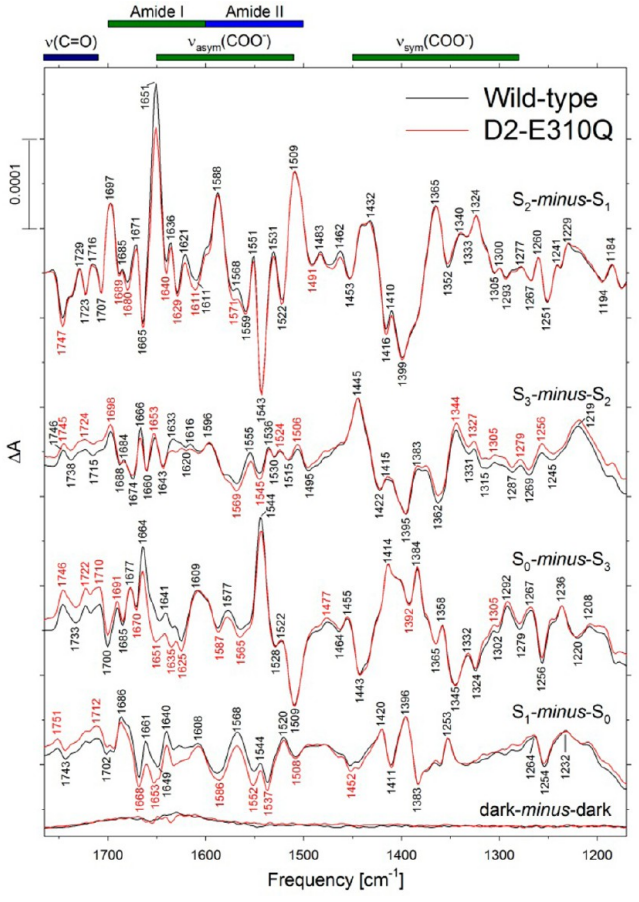

Figure 8. Comparison of the midfrequency FTIR difference spectra of wild-type (black) and D2-E310Q (red) PSII core complexes in response four successive flash illuminations applied at 0 °C. The data represent the averages of 12 wild-type and 20 D2-E310Q samples (14 700 and 26 900 scans for each trace, respectively). The spectra were normalized to maximize the overlap between 1450 and 1350 cm^{-1} by multiplying the mutant spectra vertically by a factor of ∼1.4 after normalization to the peak-to peak amplitudes of the negative ferricyanide peak at 2115 cm^{-1} and the positive ferrocyanide peak at 2038 cm^{-1}. Dark-*minus*-dark control traces are included to show the noise level (lower traces).

spectrum. Accordingly, approximately 70% of the D2-E307Q PSII core complexes were estimated to contain photo-oxidizable Mn_4CaO_5 clusters. This estimate correlates approximately with the steady-state rates of O_2 evolution observed in the mutant PSII core complexes, suggesting that those Mn_4CaO_5 clusters that assemble in the mutant are all active. After normalization, the S_{n+1}-*minus*-S_n FTIR Difference spectra of the D2-E310Q PSII core complexes closely resembled the corresponding spectra of wild type. Differences include a smaller amplitude peak at 1651 cm^{-1} in the S_2-*minus*-S_1 spectrum, more pronounced negative features at 1651 and 1635 cm^{-1} in the S_0-*minus*-S_3 spectrum, and an upshift to 1653 cm^{-1} and increased intensity of the negative feature at 1649 cm^{-1} in the S_1-*minus*-S_0 spectrum. Of particular importance to this study, the features at 1746 cm^{-1} in the S_2-*minus*-S_1, S_3-*minus*-S_2, and S_0-*minus*-S_3 spectra and the derivative feature at 1751(+)/1743(−) cm^{-1} in the S_1-*minus*-S_0 spectrum were unaffected by the D2-E310Q mutation with the exception of a 1 cm^{-1} downshift of the positive feature at 1746 cm^{-1} in the S_3-*minus*-S_2 spectrum.

D2-E323Q Mutant. Cells of the D2-E323Q mutant were photoautotrophic and evolved O_2 at 350−400 μmol O_2 (mg of Chl)$^{-1}$ h^{-1} under light-saturating conditions compared to 570−580 μmol O_2 (μg of Chl)$^{-1}$ h^{-1} for wild-type cells. The O_2-evolving activities of the D2-E310Q PSII core particles were approximately 2.9 mmol O_2 (mg of Chl)$^{-1}$ h^{-1} compared to 5.3−5.7 mmol O_2 (mg of Chl)$^{-1}$ h^{-1} for wild type. The O_2-evolving activity of the D2-E310Q PSII core complexes (approximately 53% compared to wild type) correlated approximately with the O_2-evolving activity of D2-E310Q cells (60−70% compared to wild type). The midfrequency FTIR difference spectra of wild-type and D2-E332Q PSII core complexes that were induced by four successive flashes are compared in Figure 9 (black and red spectra, respectively). When the amplitudes of the spectra were normalized to the extent of flash-induced charge separation, the amplitudes of the D2-E323Q spectra were approximately 90% of the amplitude of the wild-type spectrum. Accordingly, approximately 90% of the D2-E323Q PSII core complexes were estimated to contain photo-oxidizable Mn_4CaO_5 clusters. The lower steady-state

dx.doi.org/10.1021/bi401450y | *Biochemistry* 2014, 53, 1001−1017

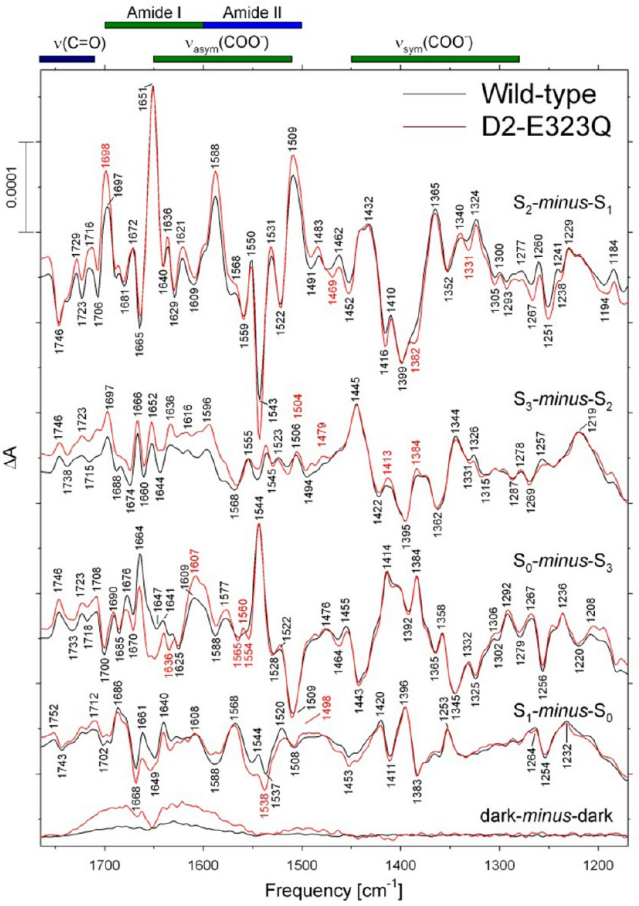

Figure 9. Comparison of the midfrequency FTIR difference spectra of wild-type (black) and D2-E323Q (red) PSII core complexes in response four successive flash illuminations applied at 0 °C. The data represent the averages of 12 wild-type and nine D2-E323Q samples (14 700 and 12 100 scans for each trace, respectively). The spectra were normalized to maximize the overlap between 1450 and 1350 cm^{-1} by multiplying the mutant spectra vertically by a factor of ∼1.1 after normalization to the peak-to peak amplitudes of the negative ferricyanide peak at 2115 cm^{-1} and the positive ferrocyanide peak at 2038 cm^{-1}. Dark-*minus*-dark control traces are included to show the noise level (lower traces).

rates of O_2 evolution exhibited by D2-E323Q PSII core complexes compared to their estimated content of Mn_4CaO_5 clusters suggests that the S-state transitions proceed less efficiently in the presence of the D2-E323Q mutation. After normalization, the S_{n+1}-*minus*-S_n FTIR Difference spectra of the D2-E323Q PSII core complexes closely resembled the corresponding spectra of wild type. Differences include more intense features at 1698(+),1588(+),1543(−), and 1509(+) cm^{-1} and the appearance of a negative shoulder at 1382 cm^{-1} in the S_2-*minus*-S_1 spectrum, a negative feature at 1655 cm^{-1}, more pronounced negative features at 1649 and 1636 cm^{-1}, and a more intense positive feature at 1607 cm^{-1} in the S_0-*minus*-S_3 spectrum, a negative feature at 1653 cm^{-1} and slightly more intense negative features at 1668 and 1538 cm^{-1} in the S_1-*minus*-S_0 spectrum. Of particular importance to this study, the features at 1746 cm^{-1} in the S_2-*minus*-S_1, S_3-*minus*-S_2, and S_0-*minus*-S_3 spectra and the derivative feature at 1751(+)/1743(−) cm^{-1} in the S_1-*minus*-S_0 spectrum were unaffected by the D2-E323Q mutation.

DISCUSSION

ν(C═O) Region of Wild-Type PSII in H_2O and D_2O. FTIR difference spectroscopy is an extremely sensitive tool for characterizing the dynamic structural changes that occur during an enzyme's catalytic cycle.[74,75,84,90,91] It is particularly suited for analyzing protonation/deprotonation reactions, pK_a shifts, and changes in hydrogen-bonded structures. In PSII, the vibrational modes of numerous functional groups are altered in frequency as the Mn_4CaO_5 cluster is oxidized through the S-state cycle, including many that are attributable to carboxylate residues or hydrogen-bonded water molecules.[70−72] The primary focus of this study is the region between 1790 and 1710 cm^{-1}, a region that contains the carbonyl stretching (ν(C═O)) modes of protonated carboxylate residues.[73−75] This region also contains the keto and ester C═O vibrations of chlorophyll, pheophytin, heme, and lipids.[76] Deuteration helps distinguish between these modes because it removes the weak coupling that exists between the C═O stretching and C−O−H bending modes of the COOH group. The elimination of this coupling causes the ν(C═O) mode to downshift by 4−20 cm^{-1}.[73,77−80] This D_2O-induced downshift is diagnostic for the ν(C═O) mode of protonated carboxylate residues and has been used as such in many systems, including bacteriorhodopsin,[77,92−95] rhodopsin,[96,97] bacterial reaction centers,[98−101] heme-copper oxidases,[102−105] and photoactive yellow protein.[106] Previously, we showed that the negative feature at 1746 cm^{-1} in the S_2-*minus*-S_1 FTIR difference spectrum of wild-type PSII core complexes from *Synechocystis* sp. PCC 6803 downshifts 4 cm^{-1} after exchange into D_2O.[53] In this study, we confirmed this observation. In addition, we showed that positive features at 1746 cm^{-1} in the S_3-*minus*-S_2 and S_1-*minus*-S_0 FTIR difference spectra and a derivative-shaped feature at 1751(+)/1743(−) cm^{-1} in the S_1-*minus*-S_0 FTIR difference spectrum downshift by 3−7 cm^{-1} after exchange into buffers containing D_2O. On the basis of these observations, we conclude that these features all correspond to the ν(C═O) modes of protonated carboxylate groups.

The frequency of the ν(C═O) mode of a carboxylic acid residue depends on the number and strengths of hydrogen bonds involving its C═O and O−H moieties.[73,77−80] The appearance of the features at 1746 cm^{-1} in the in the S_2-*minus*-S_1, S_3-*minus*-S_2, and S_0-*minus*-S_3 spectra and at 1751(+)/1743(−) cm^{-1} in the S_1-*minus*-S_0 spectrum suggests that each of the protonated carboxylate groups giving rise to these features participates in a single hydrogen bond that involves the C═O moiety,[79,80] although participation in two hydrogen bonds, with one involving the oxygen of the C−O−H group, cannot be excluded.[80] In an FTIR difference spectrum, the peak corresponding to the ν(C═O) mode of a protonated carboxylate residue can change in a number of ways. For example, partial protonation (deprotonation) of the carboxylate group gives rise to a single positive (negative) absorption band. Alternatively, a change in the environment of the protonated carboxylate group can shift its ν(C═O) mode, giving rise to a differential feature.

The shapes of the 1746 cm^{-1} features in the S_2-*minus*-S_1, S_3-*minus*-S_2, and S_0-*minus*-S_3 spectra imply that each corresponds to the partial protonation or deprotonation of at least one carboxylate group. On the basis of the relative amplitudes of these features, one might conclude that the carboxylic acid residue that that partly deprotonates during the S_1 to S_2 transition has its pK_a value restored during the S_2 to S_3 and

dx.doi.org/10.1021/bi401450y | *Biochemistry* 2014, 53, 1001−1017

S_3 to S_0 transitions. However, in our previous FTIR data obtained with wild-type PSII core complexes from *Synechocystis* sp. PCC 6803, these features frequently appeared at 1747 cm^{-1} in the S_2-*minus*-S_1 and S_0-*minus*-S_3 FTIR difference spectra and at 1745 cm^{-1} in the S_3-*minus*-S_2 FTIR difference spectrum (e.g., refs 53, 58, and 107). Furthermore, the 1746(+) cm^{-1} feature in our current S_3-*minus*-S_2 spectrum is downshifted to a greater extent (7 cm^{-1}) than the corresponding features in the S_2-*minus*-S_1 and S_3-*minus*-S_0 spectra (4 cm^{-1}) after exchange into D_2O. Given that the 1746(−) cm^{-1} feature in the S_2-*minus*-S_1 spectrum arises from a carboxylate group whose pK_a value decreases in response to the increased charge that develops on the Mn_4CaO_5 cluster during the S_1 to S_2 transition,[53] we propose that 1746(+) cm^{-1} feature in the S_3-*minus*-S_2 spectrum arises from a second carboxylate group whose pK_a value increases in response to the changes in the geometry of the Mn_4CaO_5 cluster that accompany[25,108−110] the S_2 to S_3 transition. In addition, we propose that the pK_a shifts giving rise to the 1746(−) cm^{-1} feature in the S_2-*minus*-S_1 spectrum and to the 1746(+) cm^{-1} feature in the S_3-*minus*-S_2 spectra are both reversed during the S_3 to S_0 transition. The amplitude of the 1746(+) cm^{-1} feature in the S_0-*minus*-S_3 FTIR difference spectrum would then reflect the larger amplitude of the 1746(−) cm^{-1} feature in the S_2-*minus*-S_1 spectrum compared to the 1746(+) cm^{-1} feature in the S_3-*minus*-S_2 spectrum. Finally, we propose that the derivative nature of the 1751(+)/1743(−) cm^{-1} feature in the S_1-*minus*-S_0 spectrum reflects a change in the environment of a third carboxylic acid group during the S_0 to S_1 transition, a change that does not change this group's pK_a value. This environmental change would be expected to reverse during the other S-state transitions. We see no evidence for such a reversal. However, the amplitude of this feature is sufficiently weak that any such reversal is probably lost beneath the larger 1746 cm^{-1} features in the other S_{n+1}-*minus*-S_n FTIR difference spectra.

D1-R334A Mutation. The D1-R334A mutation introduces perturbations throughout the amide and carboxylate stretching regions of the S_2-*minus*-S_1 FTIR difference spectrum and decreases the apparent efficiencies of the S-state transitions (i.e., increases the miss parameter) so that significant fractions of PSII centers fail to advance after each flash. Of particular importance to this study, the mutation decreased the amplitude of the negative band at 1746 cm^{-1} in the S_2-*minus*-S_1 spectrum and eliminated the positive band at 1746 cm^{-1} in the S_3-*minus*-S_2 spectrum (for an expanded view of these regions of the S_3-*minus*-S_2 and S_2-*minus*-S_1 spectra, see the left traces of Figure 10). In our earlier study, we concluded that D1-E65, D2-E312, and D1-E329 participate in a common network of hydrogen bonds, elements of which might exist only transiently, and that mutation of any of these residues eliminates the negative 1746 cm^{-1} feature from the S_2-*minus*-S_1 spectrum by disrupting this network.[53] Because the D1-R334A mutation substantially decreases the amplitude of the same feature, we conclude that D1-R334 participates in the same network. In addition, the substantially decreased efficiencies of the S-state transitions in the D1-R334A mutant, shown by the lack of spectral features in the FTIR difference spectra that were produced by the third and fourth flashes (Figure 4), are consistent with a role for D1-R334 in a dominant postulated proton-egress pathway linking the Mn_4CaO_5 cluster with the thylakoid lumen, as was concluded previously for D1-D61, D1-E65, and D2-E312 on the basis of similar FTIR data.[53] The participation of D1-R334 in a network of hydrogen bonds involving these residues is

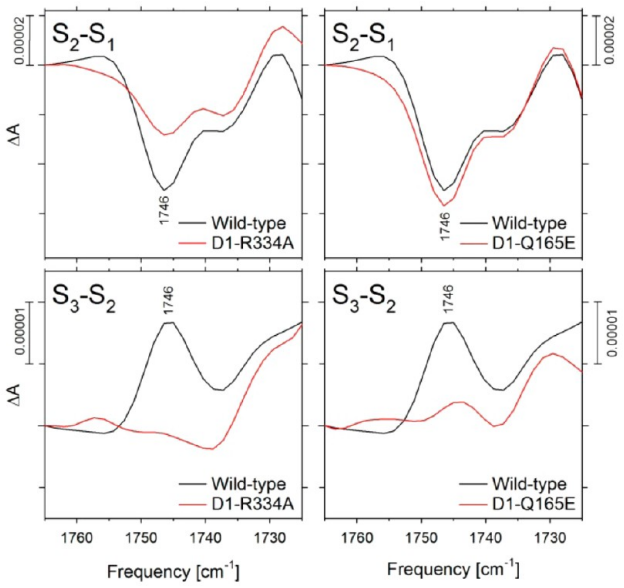

Figure 10. Comparison of the ν(C═O) regions of the S_2-*minus*-S_1 and S_3-*minus*-S_2 FTIR difference spectra of wild-type PSII core complexes (black) with the corresponding spectra of D1-R334A (red) PSII core complexes (left traces) and D1-Q165E (red) PSII core complexes (right traces). The data are reproduced from Figures 4 and 5 but were shifted vertically to coincide at 1765 cm^{-1}. Note the different vertical scales.

expected on the basis of the 1.9 Å structural model (Figure 1). In this model,[1,10] D1-R334 may form hydrogen bonds with the carboxylate groups of both D1-E65 and D2-E312. These two residues have been proposed to form hydrogen bonds with each other, comprising a carboxylate dyad whose potential importance in proton transfer has been pointed out by others.[39,40] Furthermore, on the basis of molecular dynamics simulations, it has been proposed that residues D1-D61, D1-E65, D2-E312, D1-R334, and D1-N335 form a highly interconnected network of hydrogen bonds that includes numerous water molecules, with the D1-E65/D2-E312/D1-R334 triad forming a proton-release group/proton-loading site.[40] A network of hydrogen bonds leading from the Mn_4CaO_5 cluster to the thylakoid lumen and including D1-D61, D1-E65, and D2-E312 has been inferred from the distribution of water molecules in the 1.9 Å structural model of PSII.[1,39,40] Even before the 1.9 Å structural model became available, the side chains of D1-D61, D1-E65, and D2-E312 had been proposed to participate in a proton-egress channel[34,36,41−44] having D1-E65 located at the channel's narrowest point.[36,44] As we noted previously,[53] the kinetically efficient transfer of protons through a potential channel requires finely tuned pK_a differences between key residues and the transient formation of clusters of water molecules.[111−114] Consequently, mutation of key residues in a dominant proton-egress pathway (e.g., D1-D61, D1-E65, D2-E312, and now D1-R334) would be expected to slow oxidation of the Mn_4CaO_5 cluster in the same manner that mutations that impair proton uptake slow electron transfer to from $Q_A^{\bullet-}$ to $Q_B^{\bullet-}$ in reaction centers of *Rhodobacter sphaeroides*[115−117] and the reduction of O_2 to H_2O in cytochrome *c* oxidase.[118−120]

The participation of D1-R334 in a dominant proton-egress pathway is consistent with earlier studies. In *Synechocystis* sp. PCC 6803, the D1-R334E and D1-R334 V mutations result in

dx.doi.org/10.1021/bi401450y | *Biochemistry* 2014, 53, 1001−1017

O_2 flash yields that have higher miss parameters and O_2-release kinetics that are substantially slowed compared to wild type.[121] In *Chlamydomonas reinhardtii*, the D1-R334K and D1-R334N mutations also result in altered miss parameters compared to wild type.[40] Several of the changes in the S_2-*minus*-S_1 FTIR difference spectrum of D1-R334A PSII core complexes resemble those observed previously with the mutant D1-D61A,[53] particularly the elimination of the negative feature at 1522(−) cm^{-1} and the substantial decrease in amplitudes of the features at 1588(+), 1543(−), and 1509(+) cm^{-1}.[53] Similar changes (i.e., the elimination of the 1522(−) cm^{-1} feature and the substantial decrease in amplitudes of the features at 1588(+) and 1509(+) cm^{-1}) have also been observed in mutants D2-K317A, D2-K317Q, and D2-K317E.[89] Mutations D1-D61A and D1-D61N result in O_2 flash yields that have higher miss parameters than wild type and decrease the rate of O_2 release 8- to 33-fold, respectively.[122−124] Mutations of D2-Lys317 result in O_2 flash yields that have higher miss parameters and decrease the rate of O_2 release 2- to 3-fold.[89] This residue is located in the same network of hydrogen bonds as D1-D61, D1-E65, D2-E312, and D1-R334 and coordinates to the Cl^- ion[1] that is located near D1-D61.[89,125] The elimination of the same 1522(−) cm^{-1} feature by the mutations D1-D61A, D2-K317A, and D1-R334A shows that mutating D1-D61, D2-K317, or D1-R334 to a nonprotonatable residue causes similar changes in the response of the polypeptide backbone to the positive charge that develops on the Mn_4CaO_5 cluster during the S_1 to S_2 transition, consistent with all three residues participating in a common structural element.

D1-Q165E Mutation. The D1-Q165E mutation introduces perturbations throughout the amide and carboxylate stretching regions of the S_2-*minus*-S_1 FTIR difference spectrum and slightly decreases the apparent efficiencies of the S_3 to S_0 and S_0 to S_1 transitions. This residue is located in close proximity to the Mn_4CaO_5 cluster, with the carbonyl group of its side chain apparently forming a hydrogen bond with W4, one of the two water molecules that ligate to the Ca ion (Figure 1). Consequently, the introduction of a new carboxylate group at this position could alter the $\nu_{sym}(COO^-)$ and $\nu_{asym}(COO^-)$ modes of nearby carboxylate residues (e.g., D1-E189) and alter the response of the protein environment to the charge that develops on the cluster during the S_1 to S_2 transition. The numerous mutation-induced alterations to the S_2-*minus*-S_1 spectrum are consistent with this expectation. Of particular importance to this study, the D1-Q165E mutation does not alter the negative 1746 cm^{-1} feature in the S_2-*minus*-S_1 spectrum but nearly eliminates the positive 1746 cm^{-1} feature from the S_3-*minus*-S_2 spectrum (see the right traces of Figure 10). The latter feature is also eliminated by mutations D1-D61A, D1-E65A, D1-E329Q, and D2-E312A.[53] The elimination of this feature by the D1-D61A, D1-E65A, and D2-E312A mutations might be caused by an increase in the miss parameter in these mutants. In contrast, the efficiencies of the S-state transitions appear to be unaltered by the D1-E329Q mutation.[53] Consequently, we conclude that D1-Q165 and D1-E329 participate in a common network of hydrogen bonds and that mutation of either residue eliminates the positive 1746 cm^{-1} feature from the S_3-*minus*-S_2 spectrum by disrupting this network. Because the side chain of D1-E329 is located approximately 13 Å from the side chain of D1-Q165, this network must extend at least 13 Å across face of the Mn_4CaO_5 cluster opposite from the D1-E65/D2-E313/D1-R334 triad. Because D1-E329 also participates in a network of hydrogen bonds that includes D1-D61 and the D1-E65/D2-E312/D1-R334 (ref 53 and this work), this proposed network is quite extensive. It is an open question whether elements of this proposed network exist only transiently. The participation of D1-Q165 in such an extensive network of hydrogen bonds is expected on the basis of the 1.9 Å structural model.[1,10] In this model, W4 forms hydrogen bonds with both D1-Gln165 and the phenolic oxygen of Y_Z (D1-Tyr161) and participates in an extensive network of hydrogen bonds that extends across the Mn_4CaO_5 cluster and via the Cl^- ion[1] and D2-K317 to the lumenal surface. This network includes D1-E189 and several water molecules including W3, the other water ligand of the Ca ion, and W2, one of two water ligands of the dangling Mn_{A4} ion. A possible role for D1-Q165 in a channel consisting of an extensive network of hydrogen bonds had suggested on the basis of analyses conducted before the 1.9 Å structural model became available.[36,42,44]

D2-E307Q, D2-D308N, D2-E310Q, and D2-E323Q Mutations. In the 1.9 Å structural model,[1,10] D2-E310 and D2-D308 participate in a network of hydrogen bonds that extends from the D1-E65/D2-E312/D1-R334 triad to the thylakoid lumen, with D2-E307 located nearby (Figure 1). The residue D2-E323 lies along a separate network of hydrogen bonds that also extends from the D1-E65/D2-E312/D1-R334 triad. The possible participation of these residues in networks of hydrogen bonds functioning in proton-egress channels has been noted by others on the basis of analyses of the 1.9 Å structural model[1,39] and had been noted earlier on the basis of analyses of the earlier 2.9 Å structural model.[36,44] Because the mutations D2-E310Q, D2-D308N, D2-E307Q, and D2-E323Q cause relatively few alterations to the S_{n+1}-*minus*-S_n FTIR difference spectra, we conclude that the carboxylate groups of these four residues are largely insensitive to the structural perturbations that accompany the oxidations of the Mn_4CaO_5 cluster during the S-state cycle. Because the four mutations appear to have little or no effect on the 1746 cm^{-1} features in these spectra, we conclude that the these four residues are located far from the three unidentified carboxylate groups giving rise to these features.

Possible Identities of the Carboxylate Groups. We have presented evidence (here and in ref 53) that the 1746(−) cm^{-1} feature in the S_2-*minus*-S_1 FTIR difference spectrum corresponds to a carboxylate group whose pK_a value decreases during the S_1 to S_2 transition. The structural response of PSII to the charge that develops on the Mn_4CaO_5 cluster during this transition presumably is transmitted electrostatically and through networks of hydrogen bonds. We have proposed that this structural response alters the environment of the carboxylate group responsible for the 1746 cm^{-1} feature, causing its pK_a value to decrease.[53] Because this feature is eliminated by the mutations D1-E65A, D2-E312A, and D1-E329Q, we have proposed that D1-Glu65, D2-Glu312, and D1-Glu329 participate in the same network of hydrogen bonds as the carboxylate group responsible for the 1746(−) cm^{-1} feature and that the mutation of any of these three residues to a nonprotonatable residue disrupts the network sufficiently that the structural perturbations associated with S_1 to S_2 transition are no longer transmitted to this carboxylate, thereby eliminating the 1746 cm^{-1} feature.[53] The carboxylate group that corresponds to this feature could be the side chain of D1-Glu65, D2-Glu312, or D1-Glu329 or another carboxylate residue located in the same proposed network of hydrogen bonds. It is not D1-D61 because the D1-D61A mutation does

not eliminate the feature. Some constraints on the location of the unidentified carboxylate residue are provided by our finding that the feature is unaltered by the D1-Q165E, D2-E307Q, D2-D308N, D2-E310Q, and D2-E323Q mutations. Because D1-Q165 is located across the Mn_4CaO_5 cluster from D1-D61 and the D1-E65/D2-E312/D1-R334 triad, and because D2-E307, D2-D308, D2-E310, and D2-E323 lie even farther from the Mn_4CaO_5 cluster, we conclude that the unidentified carboxylate residue must be D1-E65, D2-E312, a residue in their vicinity, or a residue between the D1-E65/D2-E312/D1-R334 triad and D1-E329 (our reason for provisionally excluding D1-E329 is given in the next paragraph). One possibility is D1-D59. The closest distance between the carboxylate oxygens of this residue and those of D1-E65 is 6.9 Å.

In this study, we also present evidence that the 1746(+) cm^{-1} feature in the S_3-*minus*-S_2 FTIR difference spectrum corresponds to a second carboxylic acid group, one whose pK_a value increases during the S_2 to S_3 transition. The structural response of PSII to the geometric changes in the Mn_4CaO_5 cluster that accompany this transition[25,108−110] presumably is transmitted through networks of hydrogen bonds, altering the environment of the carboxylate group responsible for the 1746(+) cm^{-1} feature and causing its pK_a value to increase. We propose that D1-Q165 and D1-E329 participate in a common network of hydrogen bonds and that mutation of either residue eliminates the positive 1746 cm^{-1} feature from the S_3-*minus*-S_2 spectrum by disrupting this network. The D1-Q165E mutation's disparate effect on the 1746 cm^{-1} features in the S_2-*minus*-S_1 and S_3-*minus*-S_2 spectra provides a constraint on the identity of this second carboxylate residue: it must be located closer to D1-Q165 than to the D1-E65/D2-E312/D1-R334 triad. One possibility is D1-E329 itself. The mutation D1-E329Q would then eliminate the 1746(+) cm^{-1} feature from the S_3-*minus*-S_2 spectrum directly and eliminate the 1746(−) cm^{-1} feature from the S_2-*minus*-S_1 spectrum by disrupting the network of hydrogen bonds discussed earlier in connection with the D1-R334A mutation.

We have also presented evidence that the derivative-shaped 1751(+)/1743(−) cm^{-1} feature in the S_1-*minus*-S_0 spectrum corresponds to a of a third carboxylic acid group whose environment changes during the S_0 to S_1 transition. This feature appears to be eliminated by the D1-E329Q mutation[53] but is only slightly perturbed by the D1-Q165E mutation (this work). It may correspond to another of the carboxylate groups in or near the D1-E65/D2-E312/D1-R334 triad.

SUMMARY AND CONCLUSIONS

We propose that the features observed in the ν(C=O) regions of the S_{n+1}-*minus*-S_n FTIR difference spectra of wild-type PSII core complexes from *Synechocystis* sp. PCC 6803 arise from three separate carboxylic acid groups. The pK_a value of one decreases in response to the increased charge that develops on the Mn_4CaO_5 cluster during the S_1 to S_2 transition, the pK_a value of a second increases in response to the changes in the Mn_4CaO_5 cluster's geometry that occur during the S_2 to S_3 transition, and the environment of a third becomes altered during the S_0 to S_1 transition in a manner that does not change this group's pK_a value. We have obtained experimental evidence that D1-R334 forms part of the same dominant proton-egress pathway as D1-D61, D1-E65, and D2-E312 and that D1-Q165 participates in an extensive network of hydrogen bonds that that extends across the Mn_4CaO_5 cluster to the D1-E65/D2-E312/D1-R334 triad that includes several water molecules including the W2 and W3 water ligands of the Mn_{A4} and Ca ions, respectively. Finally, we conclude that D2-E307, D2-D308, D2-E310, and D2-E323 are located far from the three unidentified carboxylate groups that give rise to the ν(C=O) features in the FTIR difference spectra.

AUTHOR INFORMATION

Corresponding Author

*Phone: (951) 827-3483. Fax: (951) 827-4294. E-mail: richard.debus@ucr.edu.

Present Address

[§]Zilkha Neurogenetic Institute, University of Southern California, Los Angeles, California 90093, United States.

Funding

Supported by the Department of Energy, Office of Basic Energy Sciences, Division of Chemical Sciences (grant DE-FG02-10ER16191 to R.J.D.)

Notes

The authors declare no competing financial interest.

ACKNOWLEDGMENTS

We are grateful to Anh P. Nguyen for maintaining the mutant and wild-type cultures of *Synechocystis* sp. PCC 6803 and for purifying the thylakoid membranes that were used for the isolation of PSII core complexes.

DEDICATION

[‖]Our close friend and colleague Warwick Hillier passed away on January 10, 2014. He was much too young and will be greatly missed.

ABBREVIATIONS

Chl, chlorophyll; DCMU, 3-(3,4-dichlorophenyl)-1,1-dimethylurea; EDTA, ethylenediaminetetraacetic acid; EPR, electron paramagnetic resonance; EXAFS, extended X-ray absorption fine structure; FTIR, Fourier transform infrared; MES, 2-(*N*-morpholino)-ethanesulfonic acid; NTA, nitrilotriacetic acid; P_{680}, chlorophyll multimer that serves as the light-induced electron donor in PSII; Pheo, pheophytin; PSII, photosystem II; Q_A, primary plastoquinone electron acceptor; Q_B, secondary plastoquinone electron acceptor; XANES, X-ray absorption near edge structure; Y_Z, tyrosine residue that mediates electron transfer between the Mn_4Ca cluster and $P_{680}^{+\bullet}$

REFERENCES

(1) Umena, Y., Kawakami, K., Shen, J.-R., and Kamiya, N. (2011) Crystal structure of oxygen-evolving photosystem II at a resolution of 1.9 Å. *Nature 473*, 55−60.

(2) Cardona, T., Sedoud, A., Cox, N., and Rutherford, A. W. (2012) Charge separation in Photosystem II: A comparative and evolutionary overview. *Biochim. Biophys. Acta 1817*, 26−43.

(3) Barber, J. (2012) Photosystem II: The water-splitting enzyme of photosynthesis. *Cold Spring Harbor Symp. Quant. Biol. 77*, 295−307.

(4) Shi, L.-X., Hall, M., Funk, C., and Schröder, W. P. (2012) Photosystem II, a growing complex: Updates on newly discovered components and low molecular mass proteins. *Biochim. Biophys. Acta 1817*, 13−25.

(5) Messinger, J., Noguchi, T., and Yano, J. (2012) Photosynthetic O_2 evolution, in *Molecular Solar Fuels* (Wydrzynski, T., and Hillier, W., Eds.) pp 163−207, Royal Society of Chemistry, Cambridge, UK.

(6) Renger, G. (2012) Mechanism of light induced water splitting in Photosystem II of oxygen evolving photosynthetic organisms. *Biochim. Biophys. Acta 1817*, 1164−1176.

(7) Dau, H., Zaharieva, I., and Haumann, M. (2012) Recent developments in research on water oxidation by photosystem II. *Curr. Opin. Chem. Biol. 16*, 3−10.
(8) Cox, N., Pantazis, D. A., Neese, F., and Lubitz, W. (2013) Biological water oxidation. *Acc. Chem. Res. 46*, 1588−1596.
(9) Cox, N., and Messinger, J. (2013) Reflections on substrate water and dioxygen formation. *Biochim. Biophys. Acta 1827*, 1020−1030.
(10) Kawakami, K., Umena, Y., Kamiya, N., and Shen, J.-R. (2011) Structure of the catalytic, inorganic core of oxygen-evolving Photosystem II at 1.9 Å resolution. *J. Photochem. Photobiol., B. 104*, 9−18.
(11) Luber, S., Rivalta, I., Umena, Y., Kawakami, K., Shen, J.-R., Kamiya, N., Brudvig, G. W., and Batista, V. S. (2011) S_1-state model of the O_2-evolving complex of Photosystem II. *Biochemistry 50*, 6308−6311.
(12) Ames, W., Pantazis, D. A., Krewald, V., Cox, N., Messinger, J., Lubitz, W., and Neese, F. (2011) Theoretical evaluation of structural models of the S2 state in the oxygen evolving complex of Photosystem II: Protonation states and magnetic interactions. *J. Am. Chem. Soc. 133*, 19743−19757.
(13) Siegbahn, P. E. M. (2011) The effect of backbone constraints: The case of water oxidation by the oxygen-evolving complex in PSII. *Chemphyschem. 12*, 3274−3280.
(14) Kusunoki, M. (2011) S_1-state Mn_4Ca complex of Photosystem II exists in equilibrium between the two most-stable isomeric substates: XRD and EXAFS evidence. *J. Photochem. Photobiol., B 104*, 100−110.
(15) Galstyan, A., Robertazzi, A., and Knapp, E. W. (2012) Oxygen-evolving Mn cluster in Photosystem II: The protonation pattern and oxidation state in the high-resolution crystal structure. *J. Am. Chem. Soc. 134*, 7442−7449.
(16) Isobe, H., Shoji, M., Yamanaka, S., Umena, Y., Kawakami, K., Kamiya, N., Shen, J.-R., and Yamaguchi, K. (2012) Theoretical illumination of water-inserted structures of the $CaMn_4O_5$ cluster in the S_2 and S_3 states of oxygen-evolving complex of photosystem II: Full geometry optimizations by B3LYP hybrid density functional. *Dalton Trans. 41*, 13727−13740.
(17) Siegbahn, P. E. M. (2009) Structures and energetics for O_2 formation in Photosystem II. *Acc. Chem. Res. 42*, 1871−1880.
(18) Yamanaka, S., Isobe, H., Kanda, K., Saito, T., Umena, Y., Kawakami, K., Shen, J.-R., Kamiya, N., Okamura, M., Nakamura, H., and Yamaguchi, K. (2011) Possible mechanisms for the O−O bond formation in oxygen evolution reaction at the $CaMn_4O_5(H_2O)_4$ cluster of PSII refined to 1.9 Å resolution. *Chem. Phys. Lett. 511*, 138−145.
(19) Siegbahn, P. E. M. (2012) Mechanisms for proton release during water oxidation in the S_2 to S_3 and S_3 to S_4 transitions in photosystem II. *Phys. Chem. Chem. Phys. 14*, 4849−4856.
(20) Rapatskiy, L., Cox, N., Savitsky, A., Ames, W. M., Sander, J., Nowaczyk, M. M., Rögner, M., Boussac, A., Neese, F., Messinger, J., and Lubitz, W. (2012) Detection of water-binding sites of the oxgyen-evolving complex of Photosystem II using W-band ^{17}O electron-electron double resonance-detected NMR spectroscopy. *J. Am. Chem. Soc. 134*, 16619−16634.
(21) Siegbahn, P. E. M. (2013) Water oxidation mechanism in photosystem II, including oxidations, proton release pathways, O−O bond formation and O_2 release. *Biochim. Biophys. Acta 1827*, 1003−1019.
(22) Navarro, M. P., Ames, W. M., Nilsson, H., Lohmiller, T., Pantazis, D. A., Rapatskiy, L., Nowaczyk, M. M., Neese, F., Boussac, A., Messinger, J., Lubitz, W., and Cox, N. (2013) Ammonia binding to the oxygen-evolving complex of Photosystem II identified the solvent-exchangeable oxygen bridge (μ-oxo) of the manganese tetramer. *Proc. Natl. Acad. Sci. U.S.A. 110*, 15561−15566.
(23) Pantazis, D. A., Ames, W., Cox, N., Lubitz, W., and Neese, F. (2012) Two interconvertable structures that explain the spectroscopic properties of the oxygen-evolving complex of Photosystem II in the S_2 state. *Angew. Chem., Int. Ed. 51*, 9935−9940.
(24) Saito, K., and Ishikita, H. (2013) Influence of the Ca^{2+} ion on the Mn_4Ca conformation and the H-bond network arrangement in Photosystem II. *Biochim. Biophys. Acta 1837*, 159−166.
(25) Glöckner, C., Kern, J., Broser, M., Zouni, A., Yachandra, V. K., and Yano, J. (2013) Structural changes of the oxygen-evolving complex in Photosystem II during the catalytic cycle. *J. Biol. Chem. 288*, 22607−22620.
(26) McEvoy, J. P., and Brudvig, G. W. (2006) Water-splitting chemistry of Photosystem II. *Chem. Rev. 106*, 4455−4483.
(27) Dau, H., and Haumann, M. (2007) Eight steps preceding O−O bond formation in oxygenic photosynthesis: A basis reaction cycle of the Photosystem II manganese complex. *Biochim. Biophys. Acta 1767*, 472−483.
(28) Dau, H., and Haumann, M. (2008) The manganese complex of Photosystem II in its reaction cycle − basic framework and possible realization at the atomic level. *Coord. Chem. Rev. 252*, 273−295.
(29) Sproviero, E. M., Gascón, J. A., McEvoy, J. P., Brudvig, G. W., and Batista, V. S. (2008) Quantum mechanics/molecular mechanics study of the catalytic cycle of water splitting in Photosystem II. *J. Am. Chem. Soc. 130*, 3428−3442.
(30) Dau, H., Limberg, C., Reier, T., Risch, M., Roggan, S., and Strasser, P. (2010) The mechanism of water oxidation: From electrolysis via homogeneous to biological catalysis. *ChemCatChem 2*, 724−761.
(31) Klauss, A., Haumann, M., and Dau, H. (2012) Alternating electron and proton transfer steps in photosynthetic water oxidation. *Proc. Natl. Acad. Sci. U.S.A. 109*, 16035−16040.
(32) McEvoy, J. P., and Brudvig, G. W. (2004) Structure-based mechanism of photosynthetic water oxidation. *Phys. Chem. Chem. Phys. 6*, 4754−4763.
(33) Ishikita, H., and Knapp, E.-W. (2006) Function of redox-active tyrosine in Photosystem II. *Biophys. J. 90*, 3886−3896.
(34) Ferreira, K. N., Iverson, T. M., Maghlaoui, K., Barber, J., and Iwata, S. (2004) Architecture of the photosynthetic oxygen-evolving center. *Science 303*, 1831−1838.
(35) Loll, B., Kern, J., Saenger, W., Zouni, A., and Biesiadka, J. (2005) Towards complete cofactor arrangement in the 3.0 Å resolution structure of Photosystem II. *Nature 438*, 1040−1044.
(36) Guskov, A., Kern, J., Gabdulkhakov, A., Broser, M., Zouni, A., and Saenger, W. (2009) Cyanobacterial Photosystem II at 2.9-Å resolution and the role of quinones, lipids, channels, and chloride. *Nat. Struct. Mol. Biol. 16*, 334−342.
(37) Barber, J., Ferreira, K. N., Maghlaoui, K., and Iwata, S. (2004) Structural model of the oxygen-evolving centre of Photosystem II with mechanistic implications. *Phys. Chem. Chem. Phys. 6*, 4737−4742.
(38) De Las Rivas, J., and Barber, J. (2004) Analysis of the structure of the PsbO protein and its implications. *Photosynth. Res. 81*, 329−343.
(39) Bondar, A.-N., and Dau, H. (2012) Exptended protein/water H-bond networks in photosynthetic water oxidation. *Biochim. Biophys. Acta 1817*, 1177−1190.
(40) Linke, K., and Ho, F. M. (2013) Water in Photosystem II: Structural, functional, and mechanistic considerations. *Biochim. Biophys. Acta 1837*, 14−32.
(41) Ishikita, H., Saenger, W., Loll, B., Biesiadka, J., and Knapp, E.-W. (2006) Energetics of a possible proton exit pathway for water oxidation in Photosystem II. *Biochemistry 45*, 2063−2071.
(42) Ho, F. M., and Styring, S. (2008) Access channels and methanol binding site to the $CaMn_4$ cluster in Photosystem II based on solvent accessibility simulation, with implications for substrate water access. *Biochim. Biophys. Acta 1777*, 140−153.
(43) Murray, J. W., and Barber, J. (2007) Structural characteristics of channels and pathways in Photosystem II including the identification of an oxygen channel. *J. Struct. Biol. 159*, 228−237.
(44) Gabdulkhakov, A., Guskov, A., Broser, M., Kern, J., Müh, F., Saenger, W., and Zouni, A. (2009) Probing the accessibility of the Mn_4Ca cluster in Photosystem II: Channels calculation, noble gas derivatization, and cocrystallization with DMSO. *Structure 17*, 1223−1234.
(45) Vassiliev, S., Comte, P., Mahboob, A., and Bruce, D. (2010) Tracking the flow of water through Photosystem II using molecular dynamics and streamline tracing. *Biochemistry 49*, 1873−1881.

(46) Vassiliev, S., Zaraiskaya, T., and Bruce, D. (2012) Exploring the energetics of water permeation in photosystem II by multiple steered molecular dynamics simulations. *Biochim. Biophys. Acta 1817*, 1671−1678.
(47) Vassiliev, S., Zaraiskaya, T., and Bruce, D. (2013) Molecular dynamics simulations reveal highly permeable oxygen exit channels shared with water uptake channels in photosystem II. *Biochim. Biophys. Acta 1827*, 1148−1155.
(48) Frankel, L. K., Sallans, L., Limbach, P. A., and Bricker, T. M. (2012) Identification of oxidized amino acid residues in the vicinity of the Mn_4CaO_5 cluster of Photosystem II: Implications for the identification of oxygen channels within the photosystem. *Biochemistry 51*, 6371−6377.
(49) Frankel, L. K., Sallans, L., Bellamy, H., Goettert, J. S., Limbach, P. A., and Bricker, T. M. (2013) Radiolytic mapping of solvent-contact surfaces in Photosystem II of higher plants. *J. Biol. Chem. 288*, 23565−23572.
(50) Ho, F. M. (2008) Uncovering channels in photosystem II by computer modeling: Current progress, future prospects, and lessons from analogous systems. *Photosynth. Res. 98*, 503−522.
(51) Ho, F. M. (2012) Substrate and proton channels in Photosystem II, in *Molecular Solar Fuels* (Wydrzynski, T., and Hillier, W., Eds.) pp 208−248, Royal Society of Chemistry, Cambridge, UK.
(52) Ho, F. M. (2012) Structural and mechanistic investigations of photosystem II through computational methods. *Biochim. Biophys. Acta 1817*, 106−120.
(53) Service, R. J., Hillier, W., and Debus, R. J. (2010) Evidence from FTIR difference spectroscopy of an extensive network of hydrogen bonds near the oxygen-evolving Mn_4Ca cCluster of Photosystem II involving D1-Glu65, D2-Glu312, and D1-Glu329. *Biochemistry 49*, 6655−6669.
(54) Chu, H.-A., Nguyen, A. P., and Debus, R. J. (1994) Site-directed Photosystem II mutants with perturbed oxygen evolving properties: 1. Instability or inefficient assembly of the manganese cluster *in vivo*. *Biochemistry 33*, 6137−6149.
(55) Debus, R. J., Campbell, K. A., Gregor, W., Li, Z.-L., Burnap, R. L., and Britt, R. D. (2001) Does histidine 332 of the D1 polypeptide ligate the manganese cluster in Photosystem II? An electron spin echo envelope modulation study. *Biochemistry 40*, 3690−3699.
(56) Faller, P., Rutherford, A. W., and Debus, R. J. (2002) Tyrosine D oxidation at cryogenic temperature in Photosystem II. *Biochemistry 41*, 12914−12920.
(57) Boerner, R. J., Bixby, K. A., Nguyen, A. P., Noren, G. H., Debus, R. J., and Barry, B. A. (1993) Removal of stable tyrosine radical D^+ affects the structure or redox properties of tyrosine Z in manganese-depleted Photosystem II particles from *Synechocystis* 6803. *J. Biol. Chem. 268*, 1817−1823.
(58) Strickler, M. A., Walker, L. M., Hillier, W., Britt, R. D., and Debus, R. J. (2007) No evidence from FTIR difference spectroscopy that aspartate-342 of the D1 polypeptide ligates a Mn ion that undergoes oxidation during the S_0 to S_1, S_1 to S_2, or S_2 to S_3 transitions in Photosystem II. *Biochemistry 46*, 3151−3160.
(59) Strickler, M. A., Walker, L. M., Hillier, W., and Debus, R. J. (2005) Evidence from biosynthetically incorporated strontium and FTIR difference spectroscopy that the C-terminus of the D1 polypeptide of Photosystem II does not ligate calcium. *Biochemistry 44*, 8571−8577.
(60) Tang, X.-S., and Diner, B. A. (1994) Biochemical and spectroscopic characterization of a new oxygen-evolving Photosystem II core complex from the cyanobacterium *Synechocystis* sp. PCC 6803. *Biochemistry 33*, 4594−4603.
(61) Boussac, A., Rappaport, F., Carrier, P., Verbavatz, J.-M., Gobin, R., Kirilovsky, D., Rutherford, A. W., and Sugiura, M. (2004) Biosynthetic Ca^{2+}/Sr^{2+} exchange in the Photosystem II oxygen-evolving enzyme of *Thermosynechococcus elongatus*. *J. Biol. Chem. 279*, 22809−22819.
(62) Lakshmi, K. V., Reifler, M. J., Chisholm, D. A., Wang, J. Y., Diner, B. A., and Brudvig, G. W. (2002) Correlation of the cytochrome c_{550} content of cyanobacterial Photosystem II with the EPR properties of the oxygen-evolving complex. *Photosynth. Res. 72*, 175−189.
(63) Yamanari, T., Kimura, Y., Mizusawa, N., Ishii, A., and Ono, T.-A. (2004) Mid- to low-frequency Fourier transform infrared spectra of S-state cycle for photosynthetic water oxidation in *Synechocystis* sp. PCC 6803. *Biochemistry 43*, 7479−7490.
(64) Debus, R. J., Strickler, M. A., Walker, L. M., and Hillier, W. (2005) No evidence from FTIR difference spectroscopy that aspartate-170 of the D1 polypeptide ligates a manganese ion that undergoes oxidation during the S_0 to S_1, S_1 to S_2, or S_2 to S_3 transitions in Photosystem II. *Biochemistry 44*, 1367−1374.
(65) Strickler, M. A., Hillier, W., and Debus, R. J. (2006) No evidence from FTIR difference spectroscopy that glutamate-189 of the D1 polypeptide ligates a Mn ion that undergoes oxidation during the S_0 to S_1, S_1 to S_2, or S_2 to S_3 transitions in Photosystem II. *Biochemistry 45*, 8801−8811.
(66) Noguchi, T., and Sugiura, M. (2002) Flash-induced FTIR difference spectra of the water oxidizing complex in moderately hydrated Photosystem II core films: Effect of hydration extent on S-state transitions. *Biochemistry 41*, 2322−2330.
(67) Glasoe, P. K., and Long, F. A. (1960) Use of glass electrodes to measure acidities in deuterium oxide. *J. Phys. Chem. 64*, 188−191.
(68) Salomaa, P., Schaleger, L. L., and Long, F. A. (1964) Solvent deuterium isotope effects on acid-base equilibria. *J. Am. Chem. Soc. 86*, 1−7.
(69) Hays, A.-M. A., Vassiliev, I. R., Golbeck, J. H., and Debus, R. J. (1998) Role of D1-His190 in proton-coupled electron transfer reactions in Photosystem II: A chemical complementation study. *Biochemistry 37*, 11352−11365.
(70) Noguchi, T. (2007) Light-induced FTIR difference spectroscopy as a powerful tool toward understanding the molecular mechanism of photosynthetic oxygen evolution. *Photosynth. Res. 91*, 59−69.
(71) Noguchi, T. (2008) Fourier transform infrared analysis of the photosynthetic oxygen-evolving center. *Coord. Chem. Rev. 251*, 336−346.
(72) Chu, H.-A. (2013) Fourier transform infrared difference spectroscopy for studying the molecular mechanism of photosynthetic water oxidation. *Frontiers Plant Sci. 4*, 146-1−146-6.
(73) Barth, A. (2000) The infrared absorption of amino acid side chains. *Prog. Biophys. Mol. Biol. 74*, 141−173.
(74) Rich, P. R., and Iwaki, M. (2005) Infrared protein spectroscopy as a tool to study protonation reactions within proteins, in *Biopysical and Structural Aspects of Bioenergetics* (Wikström, M., Ed.) pp 314−333, Royal Society of Chemistry, Cambridge, UK.
(75) Barth, A. (2007) Infrared Spectroscopy of Proteins. *Biochim. Biophys. Acta 1767*, 1073−1101.
(76) Socrates, G. (2001) *Infrared Characteristic Group Frequencies: Tables and Charts*, 3rd ed., John Wiley & Sons, Chichester, UK.
(77) Maeda, A., Sasaki, J., Shichida, Y., Yoshizawa, Y., Chang, M., Ni, B., Needleman, R., and Lanyi, J. K. (1992) Structures of aspartic acid-96 in the L and N intermediates of bacteriorhodopsin: Analysis by Fourier transform infrared spectroscopy. *Biochemistry 31*, 4684−4690.
(78) Dioumaev, A. K. (2001) Infrared methods for monitoring the protonation state of carboxylic amino acids in the photocycle of bacteriorhodopsin. *Biochemistry (Moscow) 66*, 1269−1276.
(79) Nie, B., Stutzman, J., and Xie, A. (2005) A vibrational spectral marker for probing the hydrogen-bonding status of protonated Asp and Glu residues. *Biophys. J. 88*, 2833−2847.
(80) Takei, K.-I., Takahashi, R., and Noguchi, T. (2008) Correlation between the hydrogen-bond structures and the C═O stretching frequencies of carboxylic acids as studied by density functional theory calculations: Theoretical basis for interpretation of infrared bands of carboxylic groups in proteins. *J. Phys. Chem. B 112*, 6725−6731.
(81) Noguchi, T., Ono, T.-A., and Inoue, Y. (1995) A carboxylate ligand interacting with water in the oxygen-evolving center of Photosystem II as revealed by Fourier transform infrared spectroscopy. *Biochim. Biophys. Acta 1232*, 59−66.

(82) Noguchi, T., and Sugiura, M. (2002) FTIR detection of water reactions during the flash-induced S-state cycle of the photosynthetic water-oxidizing complex. *Biochemistry 41*, 15706−15712.
(83) Surewicz, W. K., and Mantsch, H. H. (1988) New insight into protein secondary structure from resolution-enhanced infrared spectra. *Biochim. Biophys. Acta 952*, 115−130.
(84) Barth, A., and Zscherp, C. (2002) What vibrations tell us about proteins. *Q. Rev. Biophys. 35*, 369−430.
(85) Noguchi, T., Sugiura, M., and Inoue, Y. (1999) FTIR studies on the amino-acid ligands of the photosynthetic oxygen-evolving Mn-cluster, in *Fourier Transform Spectroscopy: Twelfth International Conference* (Itoh, K., and Tasumi, M., Eds.) pp 459−460, Waseda University Press, Tokyo, Japan.
(86) Noguchi, T., and Sugiura, M. (2003) Analysis of flash-induced FTIR difference spectra of the S-state cycle in the photosynthetic water-oxidizing complex by uniform ^{15}N and ^{13}C isotope labeling. *Biochemistry 42*, 6035−6042.
(87) Kimura, Y., Mizusawa, N., Ishii, A., Yamanari, T., and Ono, T.-A. (2003) Changes of low-frequency vibrational modes induced by universal ^{15}N- and ^{13}C-isotope labeling in S2/S1 FTIR difference spectrum of oxygen-evolving complex. *Biochemistry 42*, 13170−13177.
(88) Service, R. J., Yano, J., McConnell, I., Hwang, H. J., Niks, D., Hille, R., Wydrzynski, T., Burnap, R. L., Hillier, W., and Debus, R. J. (2011) Participation of glutamate-354 of the CP43 polypeptide in the ligation of manganese and the binding of substrate water in Photosystem II. *Biochemistry 50*, 63−81.
(89) Pokhrel, R., Service, R. J., Debus, R. J., and Brudvig, G. W. (2013) Mutation of lysine 317 in the D2 subunit of Photosystem II alters chloride binding and proton transport. *Biochemistry 52*, 4758−4773.
(90) Zscherp, C., and Barth, A. (2001) Reaction-induced infrared difference spectroscopy for the study of protein reaction mechanisms. *Biochemistry 40*, 1875−1883.
(91) Berthomieu, C., and Hienerwadel, R. (2009) Fourier transform infrared (FTIR) spectroscopy. *Photosynth. Res. 101*, 157−170.
(92) Siebert, F., Mäntele, W., and Kreutz, W. (1982) Evidence for the protonation of two internal carboxylic groups during the photocycle of bacteriorhodopsin. *FEBS Lett. 141*, 82−87.
(93) Engelhard, M., Gerwert, K., Hess, B., Kreutz, W., and Siebert, F. (1985) Light-driven protonation changes of internal aspartic acids of bacteriorhodopsin: An investigation by static and time-resolved infrared difference spectroscopy using [4-^{13}C]aspartic acid labeled purple membrane. *Biochemistry 24*, 400−407.
(94) Dioumaev, A. K., Richter, H. T., Brown, L. S., Tanio, M., Tuzi, S., Saito, H., Kimura, Y., Needleman, R., and Lanyi, J. K. (1998) Existence of a proton transfer chain in bacteriorhodopsin: Participation of Glu-194 in the release of protons to the extracellular surface. *Biochemistry 37*, 2496−2506.
(95) Dioumaev, A. K., Brown, L. S., Needleman, R., and Lanyi, J. K. (1999) Fourier-transform infrared spectra of a late intermediate of the bacteriorhodopsin photocycle suggest transient protonation of Asp-212. *Biochemistry 38*, 10070−10078.
(96) de Grip, W. J., Gillespie, J., and Rothschild, K. J. (1985) Carboxyl group involvement in the meta I and meta II stages in rhodopsin bleaching: A fourier transform infrared spectroscopic study. *Biochim. Biophys. Acta 809*, 97−106.
(97) Ganter, U. M., Gärtner, W., and Siebert, F. (1988) Rhodopsin-lumirhodopsin phototransition of bovine rhodopsin investigated by Fourier transform infrared difference spectroscopy. *Biochemistry 27*, 7480−7488.
(98) Nabedryk, E., Breton, J., Hienerwadel, R., Fogel, C., Mäntele, W., Paddock, M. L., and Okamura, M. Y. (1995) Fourier transform infrared difference spectroscopy of secondary quinone acceptor photoreduction in proton transfer mutants of *Rhodobacter sphaeroides*. *Biochemistry 34*, 14722−14732.
(99) Hienerwadel, R., Grzybek, S., Fogel, C., Kreutz, W., Okamura, M. Y., Paddock, M. L., Breton, J., Nabedryk, E., and Mäntele, W. (1995) Protonation of Glu L212 following QB- formation in the photosynthetic reaction center of *Rhodobacter sphaeroides*: Evidence from time-resolved infrared spectroscopy. *Biochemistry 34*, 2832−2843.
(100) Nabedryk, E., Breton, J., Okamura, M. Y., and Paddock, M. L. (1998) Proton uptake by carboxylic acid groups upon photoreduction of the secondary quinone (Q_B) in bacterial reaction centers from *Rhodobacter sphaeroides*: FTIR studies on the effects of replacing Glu H173. *Biochemistry 37*, 14457−14462.
(101) Nabedryk, E., Breton, J., Okamura, M. Y., and Paddock, M. L. (1998) Direct evidence of structural changes in reaction centers of *Rb. sphaeroides* containing suppressor mutations for AspL213→Asn: A FTIR study of Q_B photoreduction. *Photosynth. Res. 55*, 293−299.
(102) Hellwig, P., Rost, B., Kaiser, U., Ostermeier, C., Michel, H., and Mäntele, W. (1996) Carboxyl group protonation upon reduction of the *Paracoccus denitrificans* cytochrome *c* oxidase: Direct evidence by FTIR spectroscopy. *FEBS Lett. 385*, 53−57.
(103) Lübben, M., and Gerwert, K. (1996) Redox FTIR difference spectroscopy using caged electrons reveals contributions of carboxyl groups to the catalytic mechanism of haem-copper oxidases. *FEBS Lett. 397*, 303−307.
(104) Hellwig, P., Behr, J., Ostermeier, C., Richter, O. M., Pfitzner, U., Odenwald, A., Ludwig, B., Michel, H., and Mäntele, W. (1998) Involvement of glutamic acid 278 in the redox reaction of the cytochrome *c* oxidase from *Paracoccus denitrificans* investigated by FTIR spectroscopy. *Biochemistry 37*, 7390−7399.
(105) Lübben, M., Prutsch, A., Mamat, B., and Gerwert, K. (1999) Electron transfer induces side-chain conformational changes of gluamate-286 from cytochrome bo_3. *Biochemistry 38*, 2048−2056.
(106) Xie, A., Hoff, W. D., Kroon, A. R., and Hellingwerf, K. J. (1996) Glu46 donates a proton to the 4-hydroxycinnamate anion chromophore during the photocycle of photoactive yellow protein. *Biochemistry 47*, 14671−14678.
(107) Service, R. J., Yano, J., Dilbeck, D. L., Burnap, R. L., Hillier, W., and Debus, R. J. (2013) Participation of glutamate-333 of the D1 polypeptide in the ligation of the Mn_4CaO_5 cluster in Photosystem II. *Biochemistry 52*, 8452−8464.
(108) Liang, W. C., Roelofs, T. A., Cinco, R. M., Rompel, A., Latimer, M. J., Yu, W. O., Sauer, K., Klein, M. P., and Yachandra, V. K. (2000) Structural change of the Mn cluster during the $S_2 \rightarrow S_3$ state transition of the oxygen-evolving complex of Photosystem II. Does it reflect the onset of water/substrate oxidation? Determination by Mn X-ray absorption spectroscopy. *J. Am. Chem. Soc. 122*, 3399−3412.
(109) Haumann, M., Müller, C., Liebisch, P., Iuzzolino, L., Dittmer, J., Grabolle, M., Neisius, T., Meyer-Klaucke, W., and Dau, H. (2005) Structural and oxidation state changes of the Photosystem II manganese complex in four transitions of the water oxidation cycle ($S_0 \rightarrow S_1$, $S_1 \rightarrow S_2$, $S_2 \rightarrow S_3$, and $S_{3,4} \rightarrow S_0$) characterized by X-ray absorption spectroscopy at 20 K and room temperature. *Biochemistry 44*, 1894−1908.
(110) Pushkar, Y., Yano, J., Sauer, K., Boussac, A., and Yachandra, V. K. (2008) Structural changes in the Mn_4Ca cluster and the mechanism of photosynthetic water splitting. *Proc. Natl. Acad. Sci. U.S.A. 105*, 1879−1884.
(111) Tommos, C., and Babcock, G. T. (2000) Proton and hydrogen currents in photosynthetic water oxidation. *Biochim. Biophys. Acta 1458*, 199−219.
(112) Wraight, C. A. (2006) Chance and design − proton transfer in water, channels and bioenergetic proteins. *Biochim. Biophys. Acta 1757*, 886−912.
(113) Silverman, D. N., and McKenna, R. (2007) Solvent-mediated proton transfer in catalysis by carbonic anhydrase. *Acc. Chem. Res. 40*, 669−675.
(114) Mikulski, R. L., and Silverman, D. N. (2010) Proton transfer in catalysis and the role of proton shuttles in carbonic anhydrase. *Biochim. Biophys. Acta 1804*, 422−426.
(115) Okamura, M. Y., Paddock, M. L., Graige, M. S., and Feher, G. (2000) Proton and electron transfer in bacterial reaction centers. *Biochim. Biophys. Acta 1458*, 148−163.

(116) Paddock, M. L., Feher, G., and Okamura, M. Y. (2003) Proton transfer pathways and mechanism in bacterial reaction centers. *FEBS Lett. 555*, 45−50.
(117) Wraight, C. A. (2005) Intraprotein proton transfer − concepts and realities from the bacterial photosynthetic reaction center, in *Biophysical and Structural Aspects of Bioenergetics* (Wikström, M., Ed.) pp 273−313, RSC Publishing, Cambridge, UK.
(118) Hosler, J. P., Ferguson-Miller, S., and Mills, D. A. (2006) Energy transduction: Proton transfer through the respiratory complexes. *Annu. Rev. Biochem. 75*, 165−187.
(119) Wikström, M., and Verkhovsky, M. I. (2007) Mechanism and energetics of proton translocation by the respiratory heme-copper oxidases. *Biochim. Biophys. Acta 1767*, 1200−1214.
(120) Brzezinski, P., and Gennis, R. B. (2008) Cytochrome c oxidase: Exciting progress and remaining mysteries. *J. Bioenerg. Biomembr. 40*, 521−531.
(121) Li, Z. L., and Burnap, R. L. (2002) Mutations of basic arginine residue 334 in the D1 protein of Photosystem II lead to unusual S_2 state properties in *Synechocystis* sp PCC 6803. *Photosynth. Res. 72*, 191−201.
(122) Hundelt, M., Hays, A.-M. A., Debus, R. J., and Junge, W. (1998) Oxygenic Photosystem II: The mutation D1-D61N in *Synechocystis* sp. PCC 6803 retards S-state transitions without affecting electron transfer from Y_Z to P_{680}^+. *Biochemistry 37*, 14450−14456.
(123) Clausen, J., Debus, R. J., and Junge, W. (2004) Time-resolved oxygen production by PSII: Chasing chemical intermediates. *Biochim. Biophys. Acta 1655*, 184−194.
(124) Dilbeck, D. L., Hwang, H. J., Zaharieva, I., Gerencser, L., Dau, H., and Burnap, R. L. (2012) The D1-D61N mutation in *Synechocystis* sp. PCC 6803 allows the observation of pH-sensitive intermediates in the formation and release of O_2 from Photosystem II. *Biochemistry 51*, 1079−1091.
(125) Suzuki, H., Yu, J., Kobayashi, T., Nakanishi, H., Nixon, P. J., and Noguchi, T. (2013) Functional roles of D2-Lys317 and the interacting chloride ion in the water oxidation reaction of Photosystem II as revealed by Fourier transform infrared analysis. *Biochemistry 52*, 4748−4757.